UNIVERSIDADE DE LISBOA
FACULDADE DE CIÊNCIAS
DEPARTAMENTO DE FÍSICA

Interfacial Properties of Active Matter

Pedro Miguel Didier Neta

Mestrado em Física
Especialização em Física Estatística e Não-Linear

Dissertação orientada por:
Dr. Cristovão Sousa Dias
Prof. Dr. Margarida M. Telo da Gama

2019

Abstract

From swarms of unicellular organisms to complex tissues, active matter stuns with its ability to self-organise. Swimming unicellular organisms, such as bacteria, are known to accumulate close to substrates, forming a non-equilibrium growing interface, where scale invariance and universal scaling laws of the roughness are expected. The morphology of the interface may affect the system's dynamical response. It is desirable to relate the interfacial morphology to the microscopic dynamical rules.

In this thesis we start by investigating, both theoretical and numerical, three non-equilibrium roughening models and their respective universality classes. Then we focus on our main objective, collective behaviour of active particles. We will study how self-propelled motion, rotational diffusion and density, drive the separation of two distinct phases, dilute and dense, and construct a phase diagram, for the motility-induced phase separation of the unconfined system. We then add a substrate and investigate how the interface roughness of active matter evolves with the number of deposited layers for two parameters, activity and density. Two distinct ensembles were studied, "canonical" and "grand canonical", and we found that for the "grand canonical" ensemble scaling exponents belong to the KPZQ universality class.

Keywords: Active matter; Phase separation; Universality classes

Resumo

De agrupamentos de organismos unicelulares a tecidos complexos, matéria activa impressiona com a sua capacidade de auto-organização. Sabe-se que os organismos unicelulares que têm a capacidade de auto-propulsão, como as bactérias, acumulam-se perto dos substratos, formando uma interface de crescimento fora do equilíbrio, onde se espera que exista invariância de escala e leis universais de escala. A morfologia da interface pode afetar a resposta dinâmica colectiva da matérica activa, sendo portanto fundamental relacionar a morfologia da interface com as regras da dinâmicas dos agentes microscópicos.

Nesta tese, o estudo é baseado em simulações numéricas, como tal, começamos por apresentar o método usado ao longo de toda a tese, Monte Carlo Cinético. Este método usado no estudo em causa, apresenta várias vantagens em relação a outros usados na literatura (Monte Carlo Standard e Dinâmica Molecular), como o facto de ser um método sem rejeição e ter uma dinâmica rápida que se baseia na selecção eventos. Para além destas vantagens, Monte Carlo Cinético permite ainda ter uma evolução temporal precisa dos fenómenos físicos, desde que as taxas usadas sejam iguais aos valores reais medidos experimentalmente.

De seguida investigamos, teórica e numericamente, três modelos fora do equilíbrio da deposição de partículas num substrato, sendo eles Deposição Aleatória, Deposição Aleatória com Relaxação na Superfície e Deposição Balística. Para cada um destes modelos estudamos a rugosidade em função do número de camadas depositadas. Para tal, foi analisado analiticamente a variação da rugosidade da interface para cada um dos modelos e derivado os respectivos conjuntos de expoentes característicos. Verificou-se, através de simulações numéricas, que de facto, os resultados teóricos correspondem aos resultados obtidos numericamente, concluindo que cada modelo pertence a três classes de universalidade distintas.

Estudado exemplos típicos de crescimento de interfaces fora do equilíbrio e as respectivas classes de universalidade, concentramo-nos no principal objectivo desta tese, o comportamento colectivo de partículas activas. Estudamos como actividade, a difusão rotacional e o número de partículas originam a separação em duas fases distintas que coexistem, diluída e densa. A definição da coexistência parte da medição dos histogramas de frequências de densidade, onde se existerem dois picos distintos de densidade, um de baixa densidade e outro de alta densidade, afirmamos que estamos na presença de um sistema que em as duas fases, diluída e densa, coexistem. A partir dos dados obtidos, obteve-se um diagrama de fases para a separação em fases induzida pela motilidade das partículas para um sistema não confinado. Para o estudo da interface de matéria activa, gerou-se uma faixa compacta de partículas activas num sistema não confinado, e obteve-se que o crescimento da rugosidade da interface pertence a classe de universalidade Edward-Wilkinson.

Por fim, com o objectivo de caracterizar a evolução da rugosidade para um sistema que parte de uma configuração desordenada, adicionamos um substrato e investigamos como a rugosidade da interface da matéria activa evolui com o número de camadas depositadas para dois parâmetros, actividade e densidade. Foram testadas duas condições distintas para o cescimento da interface, a primeira onde

o número de partículas é mantido fixo, e a segunda onde a densidade do *bulk* foi mantida constante, como tal variou-se o número de partículas ao longo do tempo. Para a primeira condição, verificou-se que existe uma uniformidade entre os histogramas da frequência de densidade com o sistema "infinito", mas não se verificou nenhum expoente característico do crescimento da rugosidade que pertence a nenhuma classe de universalidade conhecido. Na útlima condição, onde se varia o número total de partículas mantendo a densidade no *bulk* invariante, a rugosidade com o número de camadas depositadas crescia com os expoentes característico de KPZQ.

Palavras Chave: Matéria activa; Separação de fases; Classes de universalidade

Acknowledgements

I would like to start by manifesting my deep gratitude to my supervisor Cristovão Dias, for all the mentoring and everlasting patience through out all this year.

In addition, I would like to acknowledge the tutoring provided by Margarida Telo da Gama, improving significantly my understanding of all topics explored during this process.

I also would like to thank everyone at CFTC for all fruitful discussions and peer advices, as well as for the great working environment that allowed me to improve both as a scientist and as a person.

A collective thanks to all my office "rommies", specially to Vasco Braz, Francisco Cerdeira, and Gonçalo Paulo for the persistent good mood and sometimes unproductive discussions.

My final words go to all my friends, without naming them due to the principle of exclusion and shyness of some, and emphasise that without you it would not have been possible to end or start this journey. A deep sense of gratitude for you all!

List of Figures

Contents

Chapter 1

Introduction

Natures' complex and collective phenomena has astonished civilisations throughout the centuries. In recent years, with the development of new technologies, such as 3D-printing, investigators have been able to synthesise small scale devices that can mimic natural elements, like bacteria [1], and study them systematically, unveiling new properties and new physics. Besides the scientific self-interest and curiosity, these man-made micro-machines have the potential to cause great impact in our daily lives and in industrial applications, such as in personalised health care, environment sustainability and security.

Historically, the random motion of suspended grains of pollen in a fluid was first described by the botanist Robert Brown in 1827 [2, 3]. In 1905, Albert Einstein, motivated by this observation, studied and developed a model which considered that the random motion of the suspended particles in a fluid was a consequence of multiple collisions with the constituents of the fluid [4]. In 1926, the french physicist Jean Baptiste Perrin, was awarded the corresponding Nobel prize due to an experimental set up that confirmed Einstein's theory [5]. In honour of the observations made by Robert Brown, today this erratic motion of particles in thermal equilibrium in a fluid, is called passive Brownian motion.

Active matter consists of a collection of active particles, also known as microswimmers, that differently from passive Brownian particles, can collect energy from their surroundings and convert it into mechanical work, such as self-propulsion. Countless examples of such systems are found in Nature, such as *E.coli* or spermatozoa, or even some recent examples of man-made artificial microswimmers, like Janus particles or electromagnetic rotating robots [6, 7]. In the past ten years, this area of physics and biophysics has been gaining more and more attention from the scientific community, and some important breakthroughs in the control and understanding of active particles have been made [8, 9].

In this thesis, we aim for a comprehensive study of how biological systems and artificial active particles self-organise into swarms and form patterns. A system composed of passive colloidal particles does not form groups spontaneously, unless in the presence of external fields or strong particle interaction, since their dynamics is driven by equilibrium thermal fluctuations. This is not the case for active matter, where self-propelled Brownian particles in a crowded environment can self-organise into clusters. This spontaneous grouping of active particles into clusters gives rise to a high- and -low density non-equilibrium regions, and for that reason a system composed of microswimmers can undergo a motility-induced phase separation (MIPS) [10, 11, 12]. This phase separation only emerges as a collective phenomena, therefore steric interactions are of importance. In this thesis we will study whether active particles, subjected to an excluded volume-interaction, form clusters or not, as a function of density, activity, and rotation diffusion.

Many other biological systems are found in complex media, like spermatozoa in the presence of an oocyte, hence it is important not only to study how active matter behaves in an homogeneous envi-

ronment, but also in the presence of physical boundaries [13]. Microswimmers can evidence important interactions with solid surfaces and develop rough interfaces between the aggregated particles on the wall and the surrounding environment. A still open discussion is the universality class to which active matter interfacial growth belongs [14]. With the ambition of studying interfacial properties of active matter in a semi-confined system with planar substrates, we developed two models, a canonical and a grand canonical ensemble, and investigate possible universality classes of active matter roughening.

This thesis is organised as follows: in section 2 we introduce the Kinetic Monte Carlo Method, the numerical method used to implement the simulation of active systems, followed by section 3 where we present a study of different universality classes through numerical and analytical deposition models. In section 4 we study the phase separation of active matter dynamics in the bulk and compute the phase diagram. Still in this section, we study a case of roughness time evolution and the corresponding universal class for an active system. In next-to-last section 5, we investigate how active systems organise and their interface grows in the presence of a semi-confined planar geometry both on “canonical” and “grand canonical” ensembles. The conclusions of this thesis are presented on the final section 6, were we summarise previous results obtained from all previous sections.

Chapter 2

Computational Method

Analytical formulation and solution of complex problems in physics, such as collective behaviour of out-of-equilibrium systems, are often a hard or even an impossible task. Examples of the this obstacles are nonlinear equations that are highly dependent on the initial conditions, like the Lorentz equations, or a general solution is yet to be discovered, like the Navier-Stokes equation [15, 16, 17]. Besides the analytical obstacles, highly costing or complex experimental set ups also impose a delay in the progression of science, as we recently experienced from the time discrepancy since Einsteins theory prediction of the gravitational waves (1916) and their direct measurement in 2016 [18]. To overcome nature's, mathematical and economical obstacles, it was mandatory to create a new strategy, and that is where computational physics comes.

Computational physics, as we know it today, appeared in the 1940's with the purpose of simulating nuclear bombs and perform hydrodynamic simulations. Since then, followed by increasing computational resources and better algorithms, like molecular dynamics and lattice Boltzmann, it has expanded it's area of applications and spread to all scientific areas (chemistry, economy, social sciences, etc.), including soft matter [19, 20].

A typical example of computational advantage and effectiveness in the study of phase transitions, is the Metropolis algorithm with Standard Monte Carlo method, when applied to the Ising model magnetic phase transition as function of the temperature [21, 22]. Consider an Hamiltonian with an interaction term between first-neighbours, aligning or misaligning spins. A random particle is selected at every iteration, and if the change in the spin orientation reduces the total energy, then the spin rotation is accepted with probability 1, if it does not decrease the total energy, then it's only accepted with a probability $e^{-k_B T}$, to ensure the Boltzmann distribution. Although it was very helpful in understanding phase transitions, critical behaviour, and magnetic properties of the Ising model, from the numerical point of view, many iterations produce unsuccessful trials at low temperatures, and therefore, computational resources are wasted on the same physical microstate.

Optimise resources, like time, is of the essence, therefore new methods are developed in order to create less time consuming and more efficient computational methods to simulate physical problems. At present study of the interfacial properties of active matter, a many body problem where analytical solutions are often difficult to obtain and experiments have yet a lot to uncover, we have approached it as an *in silico* experiment using Kinetic Monte Carlo method [23], a rejection free method.

2.1 Kinetic Monte Carlo

The Kinetic Monte Carlo method (KMC) distinguishes itself from the Standard Monte Carlo because it is a rejection free algorithm with a time evolution description. A main advantage of being a rejection free algorithm is the increased speed of simulations, since by the standard method or molecular dynamics, the simulation can spend many iterations on the same physical microstate either by rejection or by requiring many iterations to leave the stable/metastable state, making the KMC more efficient. The time evolution description also presents itself as a benefit compared with the Standard Monte Carlo method, because it enables to keep track of the real physical time as long as the proper set of rates is taken into account, as it will be explained later in this chapter.

To describe any stochastic physical phenomena it is important to make some approximations, that is, assume that only a few relevant processes are what characterises the dynamics and everything else can be neglected. In KMC we start by setting the minimal physical processes (particle interactions, aggregation, death, etc.) that mimic the behaviour of the system of interest. To each possible physical process i it has to be assigned a weight W_i, that represents the rate at which an event occurs, that is, the rate at which the physical process occurs for one particle.

We will now follow the necessary steps to execute KMC, and derive the expression for the time evolution. The implementation starts by setting the desired initial conditions. After setting them, the next step in KMC is to account for all processes i, the total number of particles n_i that can realise that corresponding event. Then the rate of the process i (R_i) is calculated by multiplying the number of available events n_i by the corresponding event weight W_i (equation 2.1a). Next we sum all R_i's between all the k possible processes, obtaining the total rate of the system R_{total}. Having counted R_{total} (equation 2.1b), a random number η between $[0 : R_{total}]$ is generated from a uniform distribution and random process j is chosen as follows,

$$R_i = n_i W_i. \tag{2.1a}$$

$$R_{total} = \sum_{i=0}^{k} R_i. \tag{2.1b}$$

$$R_j < \eta < R_{j+1}. \tag{2.1c}$$

After the process j is selected, one random particle between n_j possible is chosen and performs the assigned j process. After the event occurs, the methodology is repeated recursively until a stopping condition is attained, like a timing stop condition.

As said before, one of the advantages of KMC is that it also assesses the time evolution of the physical system, but so far we haven't mentioned how to measure it. Let us define an arbitrary time increment Δt and designate $P(\Delta t)$ as the probability of no event occurring on a time interval Δt since the last event. Let us consider another arbitrary time interval δt, where the probability of occurring an event in this δt time is $R_{total}\delta t/N$, where $N = \sum_{i=0}^{k} n_i$. Knowing the probability of not having an event, then the probability of the event occurring between the time interval Δt and another arbitrary time δt, that is, between $[\Delta t, \Delta t + \delta t]$, is given by,

$$P(\Delta t + \delta t) = P(\Delta t) - P(\Delta t) R_{total} \delta t \ , \tag{2.2}$$

which can be approximated by a solvable first order ordinary differential equation, whose solution is,

$$\Delta t = \frac{-1}{R_{total}} \ln(\eta) \ \ , \ \ \eta \in]0 : 1]. \tag{2.3}$$

, where η is a random number uniformly distributed. The η comes from the fact that $P()$ has a uniform probability between 0 and 1, and is this quantity that is in inside the $ln()$ factor.

The time increment expressed in equation 2.3 is proportional to the weights and number of events at each time step. This characteristic allows us to obtain information about real time evolution, providing that the weights of the events are rescaled properly or they can be measured in a physical experiments, for example, counting the average time for an electron changing spin at a given temperature. For out of equilibrium problems, this is a great advantage because one can relate dynamical properties from the numerical simulations with laboratory experiments, validating theories and gaining insight.

Chapter 3

Non-equilibrium Roughening

Interfaces in biological systems, such as bacterial growth, exhibit interesting properties and morphologies. Even though the mechanism behind surface growth of a colony is due to local random behaviour, that can depend both on the environment and the bacteria itself, collectively it can lead to typical morphologies, hinting that there must exist some universal description of the systems [24].

To study the disorder of surface growth, roughness, or other physical property, there are many methods of analysis. In this section we mainly used two methods, discrete models and scaling concepts. The first is used in the computational model, where we assume the all driving mechanism can be reduced to a small number of control parameters on a discrete space, and other mechanisms are either ignored or included into the stochastic parameter, with the same (space and time) statistical properties of the random variable in Appendix A, [24]. The second method of analysis, scaling concept, is used in order to predict how some physical properties of the system scale. In fact, many systems that on first-hand seem unrelated, like the branching discharges from electric breakdown of air and from solid polymethyl methacrylate, can exhibit the same fractal dimensions and so they belong to the same universality class [25, 26]. Discovering to what universality class a model belongs to, reveals general behaviour and predicts general scaling relations, based only on the knowledge of the class [26]. This predictive behaviour of distinct phenomena, that seems unrelated, can give insight for understanding the underlying driving mechanisms.

In the next section we follow the work done in [24], and present the study for Random Deposition, Random Deposition with Surface Relaxation, and Ballistic Deposition, three out-of-equilibrium systems with non-trivial interface properties. We used a discrete computational model and investigate the scaling laws associated for each deposition type, both theoretically and numerically.

3.1 Random Deposition

The Random Deposition model is a simplistic growth model where particles are randomly deposited on a substrate. The model considers a discrete lattice of size L with an initial empty plane substrate. At each time step a particle is dropped from a random position above the interface height and it follows a straight vertical trajectory until it encounters a particle below its trajectory. There it stays irreversibly deposited, increasing the surface height by $h(t, j) \to h(t, j) + 1$, where $h(t, j)$ is the height of the surface at time t for the column j. When the process is repeated iteratively, the surface will grow, creating a compact structure of fully occupied columns, where each column grows independently due to the absence of horizontal interactions (see figure 3.1).

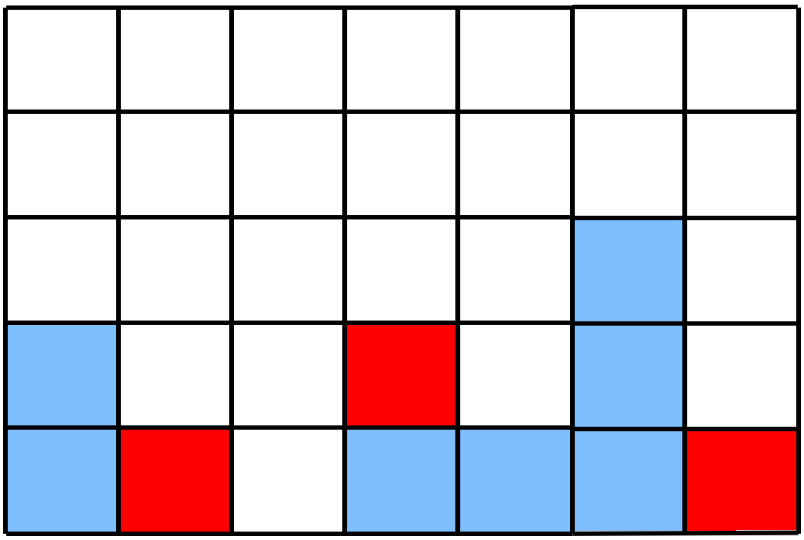

Figure 3.1: Rules of the Random Deposition model. Red blocks represent last three blocks deposited and blue the ones already deposited. Red blocks are deposited on top of the corresponding column or at the substrate if there is no column yet.

In figure 3.2, it's represented a final configuration of a computer simulation of the Random Deposition model. It is visible that the roughness grows with the number of deposited particles N, but how does it actually change? It's important to characterise this roughness. We start by defining the average height at time t as

$$\langle h(L)(t)\rangle = \frac{\sum_{i=0}^{L} h(i,t)}{L}. \tag{3.1}$$

Another important statistical quantity is the variance, given that it measures how far a set numbers are spread out from their average value. Here we define roughness $W(t)$ as the variance of the height, a quantitative measure of the average interface width relatively to its average height, and therefore,

$$W^2(t,L) = \frac{\sum_{i=0}^{L} h(i,t)^2}{L} - \langle h(L)(t)\rangle = \langle h^2(t)(L)\rangle - \langle h(t)(L)\rangle^2. \tag{3.2}$$

We are now interested on how the roughness evolves in time and wether there is an exponent characterising its growth. We start by developing an analytical expression for the time evolution of the roughness, and afterwards compare with results obtained from computer simulations to validate the developed theory.

From the set of rules described for the Random Deposition model and schematically represented on figure 3.1, we can consider the nonexistence of lateral correlations between columns. In the absence of horizontal interactions, the probability p of a column height being increased by one unit whenever a particle is deposited is $p = 1/L$. If N particles have been deposited, then the probability of a column having a determined height h must follow a binomial distribution, and therefore, the probability of having a height h after N deposited particles is,

$$P(h,N) = \binom{N}{h} p^k (1-p)^{N-h}. \tag{3.3}$$

We can then prove, by making use of the binomial theorem, that the expected value after N deposited

particles grows linearly with time, and making use of the same theorem to obtain an expression for the squared average value of the height:

$$\langle h \rangle = \sum_{h=1}^{N} hP(h,N) = Np = t \tag{3.4a}$$

and,

$$\langle h^2 \rangle = \sum_{h=1}^{N} hP(h,N) = Np(1-p) + N^2p^2, \tag{3.4b}$$

where we have redefined the timescale as the average number of deposited layers $t = N/L$.

Inserting equations 3.4 a) and b) in equation 3.2, we obtain a result that determines that the interface roughness $W(t)$ grows sublinearly with time, with a characteristic exponent $\beta = 1/2$

$$W(t) \sim t^{1/2} \tag{3.5}$$

Having developed a theoretical model for the scaling behaviour of the roughness of a growing interface in the absence of lateral interactions, as done in [24], we implemented a numerical simulation with the same set of rules as in the Random Deposition model on a discrete lattice (see figure 3.1). As we have seen, the roughness is no more than the height fluctuations of the interface, hence we need to measure the height of each column and compare it with the average height of the interface throughout the simulation. We have used the burning method technique [27], to measure the roughness of the interface, given that allows us to measure both the interface morphology and the height of each column. We also apply this technique in the next sections of active matter, and here it is only used to ensure validation of the method and future results.

For the burning method, start with a lattice with sites that are either empty or occupied, and define three distinct states for each of the occupied sites: *for burn*, *burning* and *burned*. Initially all occupied sites are set *for burn*. We start by switching states of all particles that are directly deposited onto the surface from *for burn* to *burning*. Next we search for first-neighbours of the *burning* sites and change their status from *for burn* to *burning*, and the ones that were previously *burning* are now *burned*. The process is repeated until all particles are *burned* and no particles are left *burning*. The cluster then contains all particles continuously in contact with the surface.

Having the cluster geometry formed by Random Deposition at different times, we can measure spacial and time evolution properties. Just based on visual arguments, from the representation lattice in figure *3.2*, we can observe that there is indeed an increase of the roughness with time, since the interface gets less and less uniform with the number of deposited layers. For a more precise analyses, from the plot in figure 3.3 we can verify that indeed the roughness W increases sublinearly with the number of deposited layers, with the exponent β given by equation 3.5, validating both analytical and numerical results. We can also expect the roughness to increase indefinitely with the same power law since that are no lateral correlations and therefore, no arguments for the system to change regimes.

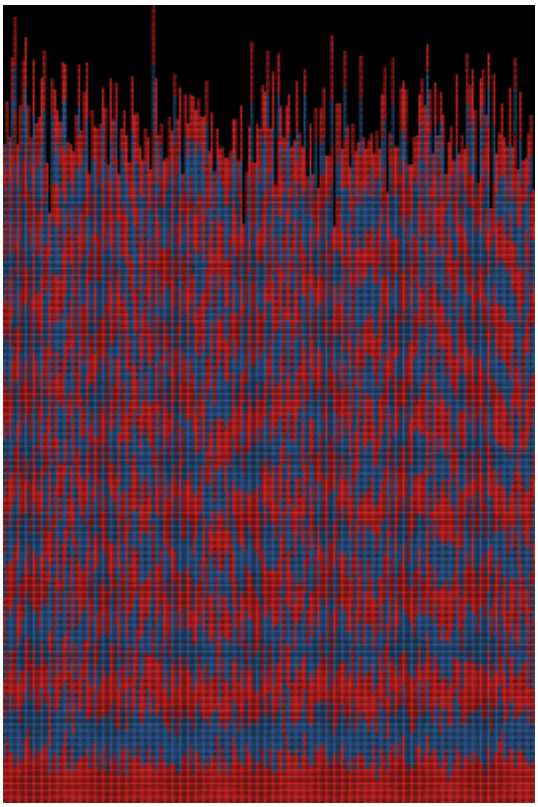

Figure 3.2: Snapshot of the final configuration for the Random Deposition model for a lattice of size L=200. Colours correspond to layers of size 20L particles.

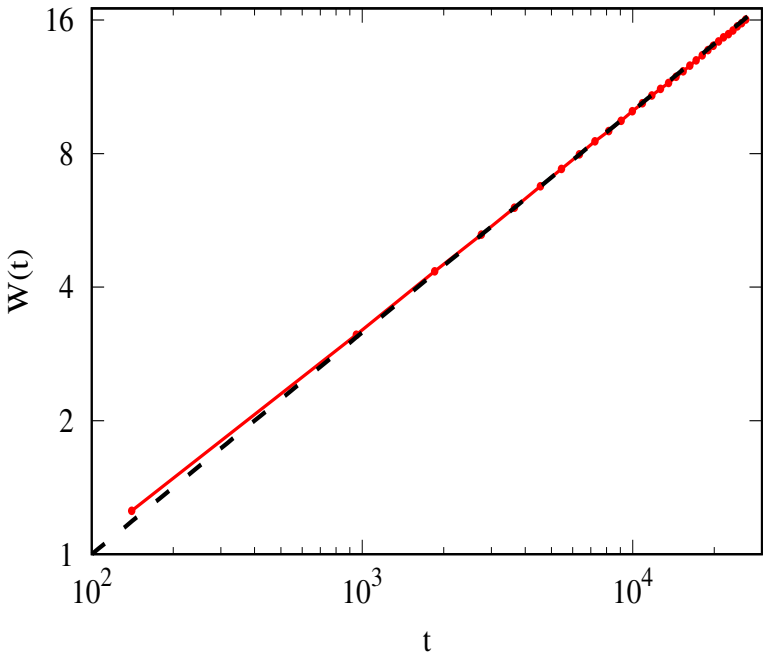

Figure 3.3: Roughness W as a function of time t (measured in terms of deposited layers) for the Random Deposition model on a lattice of size $L = 200$. Black dotted line represents $f(t) \sim t^{\frac{1}{2}}$

3.2 Random Deposition with Surface Relaxation

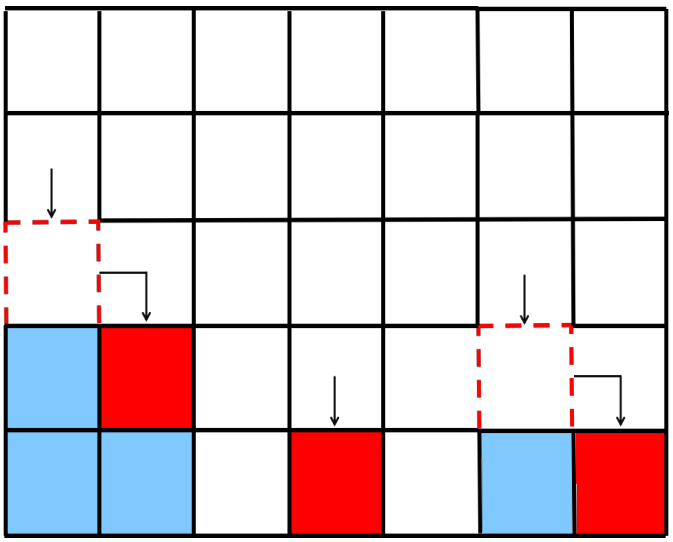

Figure 3.4: Rules for Random Deposition with Surface Relaxation. Red blocks represent the last three blocks deposited and blue ones those already deposited. Red blocks fall upon one column and if a neighbouring column has a lower height then diffuses to it.

In this section we will present the Random Deposition with Surface Relaxation model in 1+1 dimensions as in [24], and study it both analytically and numerically, by demonstrating its universal class using mathematical and symmetry arguments, and implement a numerical simulation to compare the system properties with the analytical derived expression.

Consider the Random Deposition model introduced in the previous section where particles simply fall on a column and stick irreversibly to the surface. Now, once the particle is deposited, we add to the dynamics surface relaxation, that is, instead of sticking irreversibly to the surface, the particle can diffuse along the interface one lattice space if and only if the neighbouring column has a lower height. In the eventuality of both neighbouring sites having the same height, one of the adjacent positions will be chosen at random. The inclusion of the diffusion in the model imposes lateral correlation of the order of a lattice spacing cell, minimising the local height of the interface and smoothing its roughness, as is visible from the contrast of the roughness time evolution on figures 3.5 and 3.2.

In the previous section we found a power law relation between the number of deposited layers and the increase of the roughness, displayed in equation 3.5. In this model, since the roughness has a clearly distinct behaviour, as observed from the snapshots, it must follow a distinct relation and consequently must belong to a different universality class.

We will start by describing a general growing interface by an equation as general as possible, then, by symmetry arguments, we will arrive at a simplistic equation with characteristic scale exponents, indicating a different universality class from the previous one. In fact we observed that the derived scaling relations that describe the Random Deposition with Surface Relaxation model are consistent with the numerical results.

Assume that time evolution of the interface height is a sum of two terms, one a very generic function $G(\mathbf{x},\mathbf{t},t)$ that depends on the spatial coordinate $\mathbf{x}$, on the height of the interface $\mathbf{h}$, and time t, and the second a stochastic variable η that is uncorrelated both in time and space, as explained in Appendix A. Translating into a mathematical expression it gives,

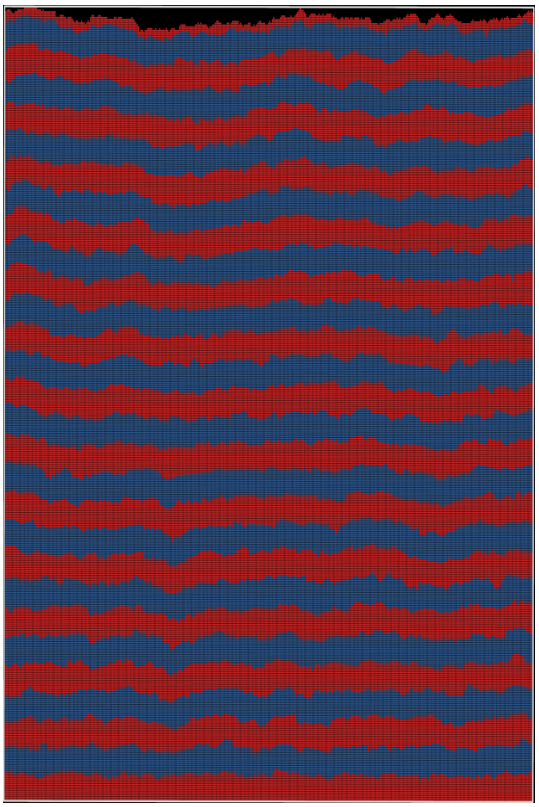

Figure 3.5: Snapshot of the final configuration for the Random Deposition with Surface Relaxation model of a lattice of size $L = 200$. Colours correspond interval of 20 layers.

$$\frac{\partial \mathbf{h}(\mathbf{x},t)}{\partial t} = G(\mathbf{x},\mathbf{h},t) + \eta(\mathbf{x},t) \tag{3.6}$$

We can now make use of five symmetry arguments about the behaviour of the interface that allow us to reduce and simplify the physical problem.

The first symmetry we use is invariance under time translation. The height of the interface should not depend on when you set your time, therefore, the system is invariant under the transformation $t \to t + \delta t$. This symmetry removes the explicit time dependence in the G function.

Another symmetry we can apply is translation invariance along the growth direction. Let's set the initial height for particles to deposit at some arbitrary height h_0 and let the interface grow. If we now change the frame of reference of the deposition surface by some constant δh, that is, change from $h_0 \to h_0 + \delta h$, the interface properties shouldn't change, hence equation 3.6 should be invariant under this transformation and cannot depend explicitly on h, although it can still be a function of any order n of $\nabla^n h$.

The height evolution of the interface should not be a local property since particles fall randomly throughout the substrate, consequently G should not depend on the actual coordinate x. This symmetry, the translation invariance in the direction perpendicular to the growth, implies that equation 3.6 must be invariant under the transformation $x \to x + \delta x$, and so G cannot depend explicitly on x.

The fourth argument that allows to simplify the time evolution of the height of the interface is the rotation and symmetry invariance in the growth direction. Consider rotating the system or growing the height in the inverse direction, then the behaviour of the interface and of the height should remain invariant, therefore the odd order terms of the gradient ($\nabla^{2n+1}h$ or $\nabla^{2n+1}(\nabla^{2n}h)$) should be excluded

from equation 3.6.

The final argument used is an up/down symmetry of h. Consider the mean height of the interface and its fluctuations. Relatively to the mean height, the positive and negative fluctuations should be similar, that is, when observed from above or from below the interface should be identical. This implies that the system should be invariant under the transformation $h \to -h$, removing the dependence on the even terms of the gradient $(\nabla h)^{2n}$.

Taking all the symmetries into consideration, the shortened and simplest version of the time evolution of the height of the interface is:

$$\frac{\partial h(\mathbf{x},t)}{\partial t} = \sum_n \nabla^{2n} h + \sum_{k,j} \nabla^{2k} h (\nabla h)^{2j} + \eta(\mathbf{x},t) \tag{3.7}$$

We are interested in the macroscopic behaviour and scaling properties of the interface and height, therefore we must study them in the long-time and long-distance limits ($t \to \infty$; $x \to \infty$). In these limits, terms of fourth order or higher order can be disregarded, since when compared with second order terms they are negligible [24]. As a result of this approximation, we obtain a final simplified expression of equation 3.7, also known as the Edward-Wilkinson (EW) equation:

$$\frac{\partial h(\mathbf{x},t)}{\partial t} = \nabla^2 h + \eta(\mathbf{x},t). \tag{3.8}$$

Even though its possible to solve the EW equation analytically, in this thesis we focused on a more intuitive technique by making use of a scaling approach, as in [24].

Consider the interface being self-affine, that is, independent of the scale in which we observe it. Since we are on the long-time, long-distance limits and the interface is self-affine, then we can rescale the spatial coordinate x and the height h by an arbitrary constant b , so that all the statistical macroscopic properties, such as the interface roughness, must remain indiscernible upon the transformation. We are interested not only on the spatial properties of the interface, but also on its time evolution t, that must also be invariant upon an arbitrary time rescale. Considering the rescale as arbitrary, assume $\mathbf{x}$ is rescaled by a constant b, and $\mathbf{h}$ and t by some powers of b, that is:

$$\mathbf{x} \to \mathbf{x}' \equiv b\mathbf{x}, \quad \mathbf{h} \to \mathbf{h}' \equiv b^{\alpha}\mathbf{h}, \quad t \to t' \equiv b^{z} t. \tag{3.9}$$

Since the physical nature of the problem cannot change after the rescaling, then equation 3.8 must remain invariant under this transformation of coordinates. Introducing the rescaled quantities in equations 3.9 in equation 3.8 and multiplying on both sides by b^{z-a}, we have:

$$\frac{\partial \mathbf{h}}{\partial t} = b^{z-2}\nabla^2 \mathbf{h} + b^{-d/2+z/2-\alpha}\eta(\mathbf{x},t), \tag{3.10}$$

where d is the dimension. By construction of the problem, the equation must be independent of the rescaled quantity b, so all terms on the r.h.s of the equation must be such that their exponents are zero.

$$z-2=0 \quad , \quad \frac{-d+z}{2} - \alpha = 0. \tag{3.11}$$

As for the exponent for the time evolution of the roughness, we know by definition and from equation 3.2 the relaxation between roughness and height. Using equation 3.8, solving $W^2 = \langle h^2 \rangle - \langle h \rangle^2$, we are left with a power law with a characteristic exponent β relating the roughness and time.

$$W \sim t^{\frac{2-d}{4}} \implies \beta = \frac{2-d}{4}. \tag{3.12}$$

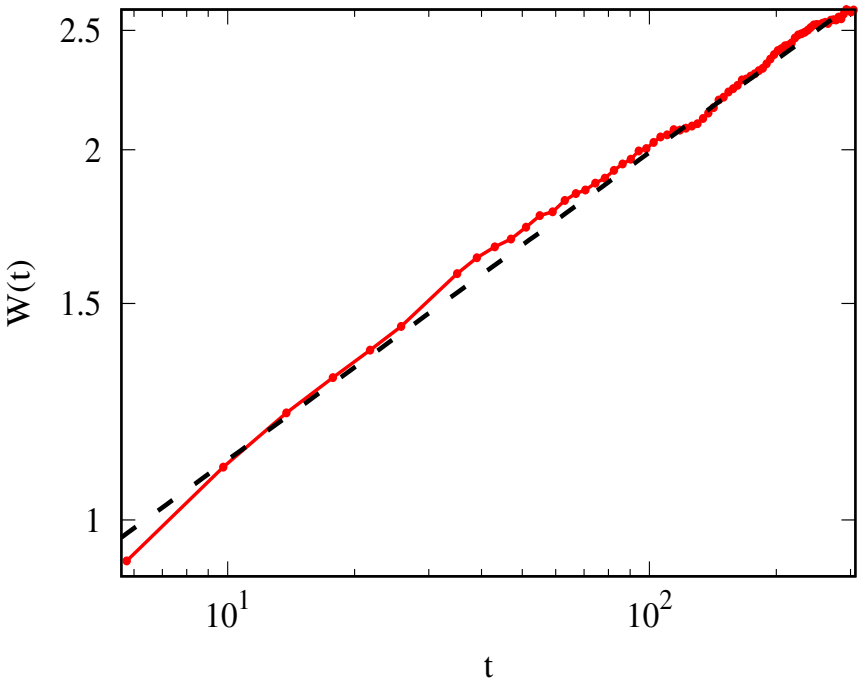

Figure 3.6: Roughness W as a function of time t measured in terms of deposited layers for the Random Deposition with Surface Relaxation model on a lattice of size $L = 200$. Black dotted line represents $f(t) \sim t^{\frac{1}{4}}$

Doing numerical experiments in one dimension ($d = 1$) of the Random Deposition with Surface Relaxation model in a discrete space, we observe from figure 3.6, that in fact this model falls into the EW universal class, since the β exponent matches with the time evolution of the roughness. For a more precise characterisation of the model and its universal class, we should perform simulations for different system sizes and confirm that the roughness growth rescaled by the system sizes to the power of α and z collapse in the same line.

We observed for a number of deposited layers lower than $\simeq 1$ that there is a misfit between the model and the numerical roughness growth. This initial misfit of the growth of the roughness from the exponent, is characteristic of the randomness of the deposited layers, since when the number of deposited layers is less than 1, particles are deposited like to the Random Deposition without surface relaxation.

3.3 Ballistic Deposition

In the final section of Non-Equilibrium Roughening models, we will address the Ballistic Deposition model and its difference from the Random Deposition and Random Deposition with Surface Relaxation. As in the three models presented previously, particles are introduced on the lattice in a random column from the L possible ones and a particle is left to move vertically from the top of the lattice. The distinct feature of Ballistic Deposition is in the dynamics of the falling bodies, where in this case we introduce lateral first-neighbour interactions, making particles aggregate as soon they find an occupied neighbouring site, either it is a vertical or a horizontal neighbour.

Imposing lateral growth correlations, alters the growth process of the interface, promoting open spaces in the columns, consequently reducing the compactness of the film. Through visual comparison of both snapshots of Random and Ballistic deposition, figures 3.2 and 3.8 respectively, we clearly observe differences between the interface roughness, were the Ballistic Deposition model has a less rough

interface compared with Random Deposition. In the Random Deposition model, a fluctuation in the increasing height of a column is only smoothed when all the interface increases size, while in in the Ballistic Deposition model, neighbouring sites smooth the fluctuation in the local height of the interface due to local horizontal growth.

The time evolution equation of the interface heights is in all similar to the expression derived for the Random Deposition with Surface Relaxation, the EW equation (3.8), but a perpendicular growth relatively to the deposit orientation is added. Local normal growth removes the up-down symmetry of the previous model, therefore we must account for the terms of the $(\nabla h)^{2n}$. The equation of the height of the interface is a result of the sum of the EW equation plus the first order therm of the removed symmetry.

$$\frac{\partial h(\mathbf{x},t)}{\partial t} = \nabla^2 h + \frac{1}{2}(\nabla h)^2 + \eta(\mathbf{x},t). \tag{3.13}$$

This smoothing of the heights induces a smaller increase rate of the surface roughness with time, and therefore the exponent associated with it should be smaller than the one from Random Deposition. In figure 3.9 we plot the time evolution of the roughness for the Ballistic Deposition model and we observe that in fact the scaling relation is approximately $W(t) \sim t^{\frac{1}{3}}$, a good approximation to the theoretical value. The fact that the Ballistic Deposition model presents a different roughening exponent, reveals it belongs to a different universality class, the Kardar-Parisi-Zhang (KPZ) universal class [24, 28]. Once again we observe different regimes in the growing interface, the initial regime associated with the randomised particle deposition, as explained in the previous section, a growing regime characteristic of the Ballistic deposition, and a saturation regime where the roughness doesn't increase and remains constant. The last regime, the saturation one, is associated with finite size effects, due to the fact that roughness does not increase since the correlation between particles is of the order of the system size L.

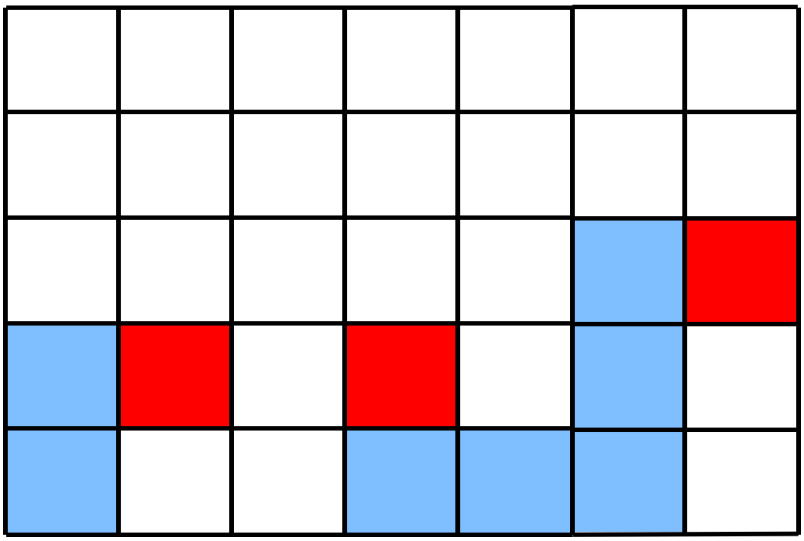

Figure 3.7: Rules of Ballistic Deposition model. Red blocks represent the last three blocks deposited and blue the ones already deposited. Red blocks deposit when they encounter a first neighbour.

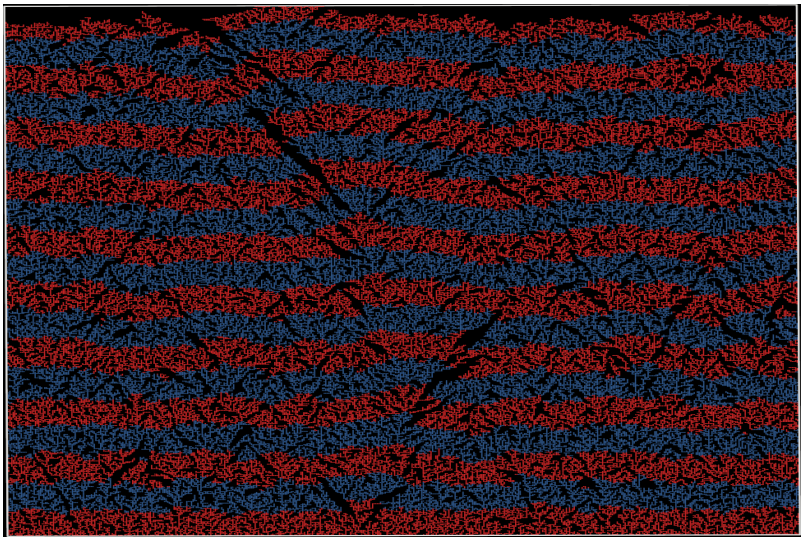

Figure 3.8: Snapshot of the final configuration for the Ballistic Deposition model for a lattice of size L=500. Colours correspond to layers of size 20L particles.

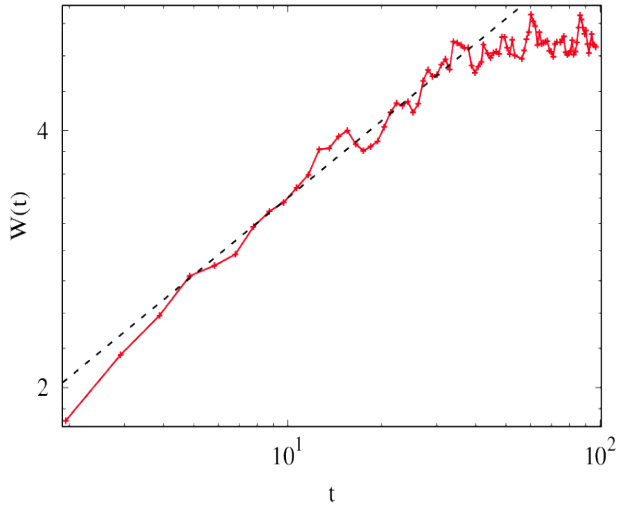

Figure 3.9: Roughness W as a function of time t measured in terms of deposited layers for the Ballisitic Deposition model on a lattice of size 500. Black dotted line represents $f(t) \sim t^{\frac{1}{3}}$.

Chapter 4

Bulk

In the previous sections we presented three different non-equilibrium roughening models, in which the responsible mechanism for interfacial growth was dropping objects with at most first neighbours interactions. In the present chapter, we aim to understand a more complex non equilibrium system, composed of active particles in a non confined space. With that goal in mind, we study numerically the motility induced phase separation (MIPS) of a 2D open discrete system of active brownian particles. Particles occupy one lattice space and interact only via excluded volume, therefore, no external fields are applied and particles do not have any pair potential besides the excluded volume.

Active microswimmers have an anisotropic motion due to an intrinsic preferential direction in which they propel, therefore, they diffuse both thermally and ballistically. Particle thermal diffusion arises from multiple collisions with the fluid in which they are suspended, causing the usual stochastic Brownian dynamics, and ballistic diffusion is originated from the self-propelled motion typical of active matter. Besides translational diffusion, microswimmers also diffuse rotationally due to the turning of their self-propelled direction in time. In the following sections we present the constructed algorithm and on section 4.2 we show the results obtained from the model. In the final section 4.3, we study the universality class of a particular roughening time evolution of active matter.

4.1 Numerical Model

Based on KMC method described on section 2.1, we performed simulations on a discrete square lattice of size L, with N self-propelled hard particles inserted randomly, each one with a random orientation, setting the density $\rho = \frac{N}{L^2}$. To each individual particle is initially assigned a vector randomly oriented to a neighbouring site. One particle, at each time step, can perform one of three processes: move to a neighbouring site due to thermal fluctuations, or due to the self-propelled motion, or diffuse rotationally by changing the vector that represents its orientation by an angle of $\frac{\pi}{2}$, condition that adds short-time memory to the system. An example of a lattice is represented on figure 4.1 with a schematic representation of the possible events for each active particle.

The dynamics of KMC is based on event selection, as shown in section 2.1, and to select the appropriate event it's necessary to calculate the rate of each process of the system at each time step. These rates must represent the balance between the distance covered by a microswimmer in the self-propulsion direction, the diffusion due thermal fluctuations and the time necessary to change the direction of active self-propelled motion.

It is known that thermal diffusion is proportional to the Bolztmann constant k_BT through the Einstein's relation [29], hence we can set the rate responsible with diffusion to $\xi = k_BT$. Self-propelled

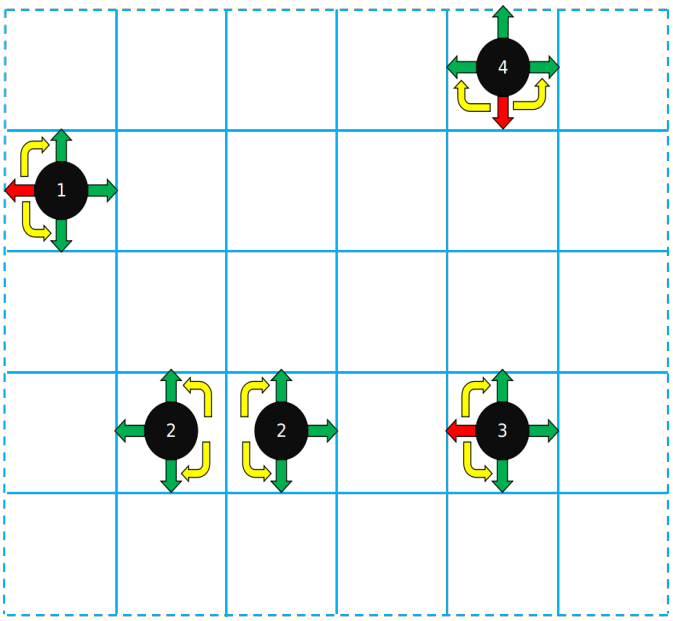

Figure 4.1: Representation of an open lattice of size 6×5 with 5 active particles. The limits marked with dashed blue lines represent the periodic boundary conditions. Each particle has green, red and yellow arrows representing non-preferential motion, preferential motion and rotation, respectively. If a particle has an occupied neighbouring site, the arrow that accounts for the motion in the occupied neighbouring direction is removed, but the yellow arrow is kept to maintain the possibility for particle rotation even in a clustering condition. Particles at each time step can either move one lattice space or rotate. In this representation, we observe that particles 2 form a small cluster since their dynamics is restricted due to the presence of other particles. If particles have a high rate of activity, then particle 3 is likely to reach the cluster formed by the 2's, and therefore decreases the freedom of motion of the system, by increasing the number of particles forming a cluster.

motion is an anisotropy of the individual dynamics leading the microswimmers to move in a superdiffuse regime, so we can estimate the rate associated to self-propulsion as an increase of thermal diffusion by a coefficient γ, setting the rate of active motion to $\varepsilon' = \xi + \gamma$. As for the rotation rate, we set it as D_r', a rate that must also be proportional to k_BT[30].

Since all rates are either proportional to k_BT or a linear combination of it, we can rescale all rates by k_BT, simplifying the results interpretation and facilitating a possible contact with an experimental group since all units are rescaled by the effective temperature. Having rescaled the rates, we set them as:

- $\xi \to \frac{k_BT}{k_BT} = 1$;
- $\varepsilon' \to \frac{\xi+\gamma}{k_BT} = 1 + \frac{\gamma}{k_BT} = \varepsilon$;
- $D_r' \to \frac{D_r'}{k_BT} = D_r$;

ε will then represent the activity parameter, and in the asymptotic limit of $\varepsilon = 1$, we recover the passive Brownian dynamics, and in the other limit of $\varepsilon \gg 1$, particles will move persistently and almost exclusively in the self-propelled direction.

Following the method presented in section 2.1, the total rate of the system at time t is the sum of all the total rates of each of the three possible processes

$$R_{total} = 2ND_r + N_- + N_+\varepsilon, \tag{4.1}$$

where N_+ represents the number of particles that can move in the self-propulsion direction and N_- the number of particles that can move in a non-preferential direction. Regarding the rotation events, in

this model we allow for every particle to rotate both clockwise and counterclockwise at any time, as represented in figure 4.1, for that reason D_r is multiplied by $2N$. After determining R_{total}, a random process is chosen with probability r_t/R_{total}, where r_t is the rate of the process r at time t. After selecting a process at random, a randomly selected particle realises an event and the system is updated, process rates are recalculated and the procedure is repeated iteratively until a stopping time.

Time evolution follows the description of section 2.1. Attributing values for every rate and counting the number of particles allowed to perform each process, time is incremented after one event is executed as in equation 2.3.

To investigate how active matter evolves from a single phase to a phase separation, the first defined as particles uniformly distributed, and the second by the simultaneous presence of dilute regions and a highly dense region, we performed simulations for different system densities (ρ), activities (ε) and rotation rates (D_r). We also investigate how possible finite size effects affect the phase separation, by covering the same parameter space for three distinct system sizes.

4.2 Results

Knowing that in the limit of activity $\varepsilon = 1$ we should recover the passive brownian motion where particles are uniformly distributed in space, we study how the activity changes the density profile of the system.

The heuristic argument for activity changing the density profile arises from flux arguments. When two particles meet and become neighbours, it restrains the dynamics by reducing possible movements of both particles. If the time scale for one of the two particles to rotate and move to an adjacent site, either by ballistic or by thermal diffusion, is smaller than the time scale for a third particle to run into one of the two, a small cluster of three particles is formed. Considering the individual motion of the three particles, each one of them is more constrained in their dynamics after clustering than when isolated. The main mechanism leading to clustering is activity, since if we have a high active rate, the system tends to choose events where particles move persistently in one direction. Now we must analyse which behaviour is the dominant one: self-propelled motion or thermal and/or rotational diffusion. If the dominant dynamics is self-propelled motion with particle collision, then many small clusters emerge and as times evolves, the small clusters rearrange until a single large cluster is formed, establishing a dense region where particles aggregate on the interface and confine particles in the interior, separating the dense and dilute phases (*vide* figure 4.2). If on the other hand, the dominant behaviour is thermal and/or rotational diffusion, then the system tends to have homogeneously distributed particles, and thus the system remains in the dilute state.

The number of active particles in the ensemble will also play a relevant role in phase transitions, like in classical equilibrium thermodynamics. Consider a very dilute ensemble where the distance between particles is of the order of the system size then, independently of the activity, particles are unlike to encounter one another and clusters will not form. On the other hand, if we have a high density lattice, then particles will collide frequently and a small activity will lead to the clustering of particles. The point of interest is to find the threshold of activities to a corresponding fixed density at which at least one dense cluster emerges.

In this section we present the characterisation of the phase space, allowing to determine how the system density and activity lead to MIPS of active matter in finite periodic system. Throughout and unless stated otherwise or explicitly shown, all results correspond to a KMC time $t = 2^{18}$.

We started by measuring the density frequency histogram in a square system of size $L = 200$ for

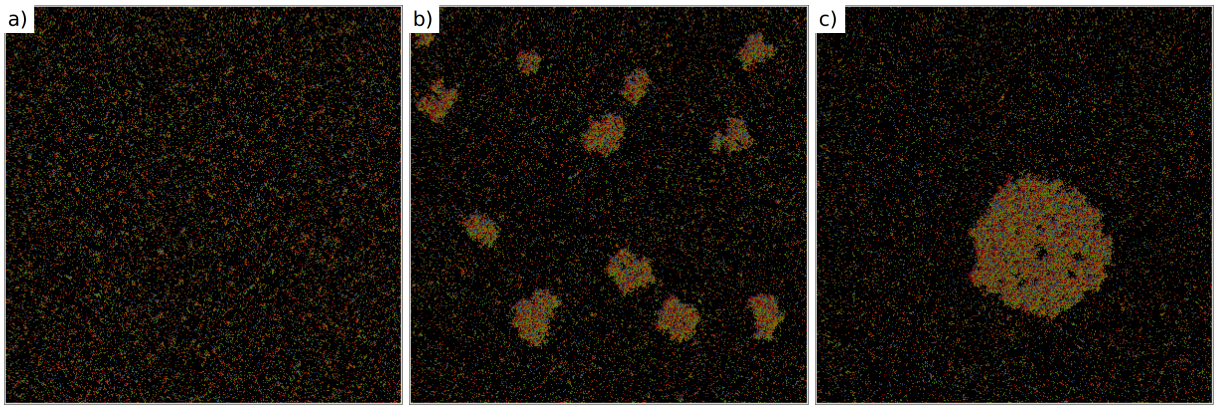

Figure 4.2: Snapshots of the time evolution, in KMC time units, of an active system where the dominant behaviour is self-propelled motion with particle collision, for a density $\rho = 0.2$ and activity $\varepsilon = 8$. a) t = 2^1; b) t = 2^9; c) t = 2^{18}; Colours represent particle orientation.

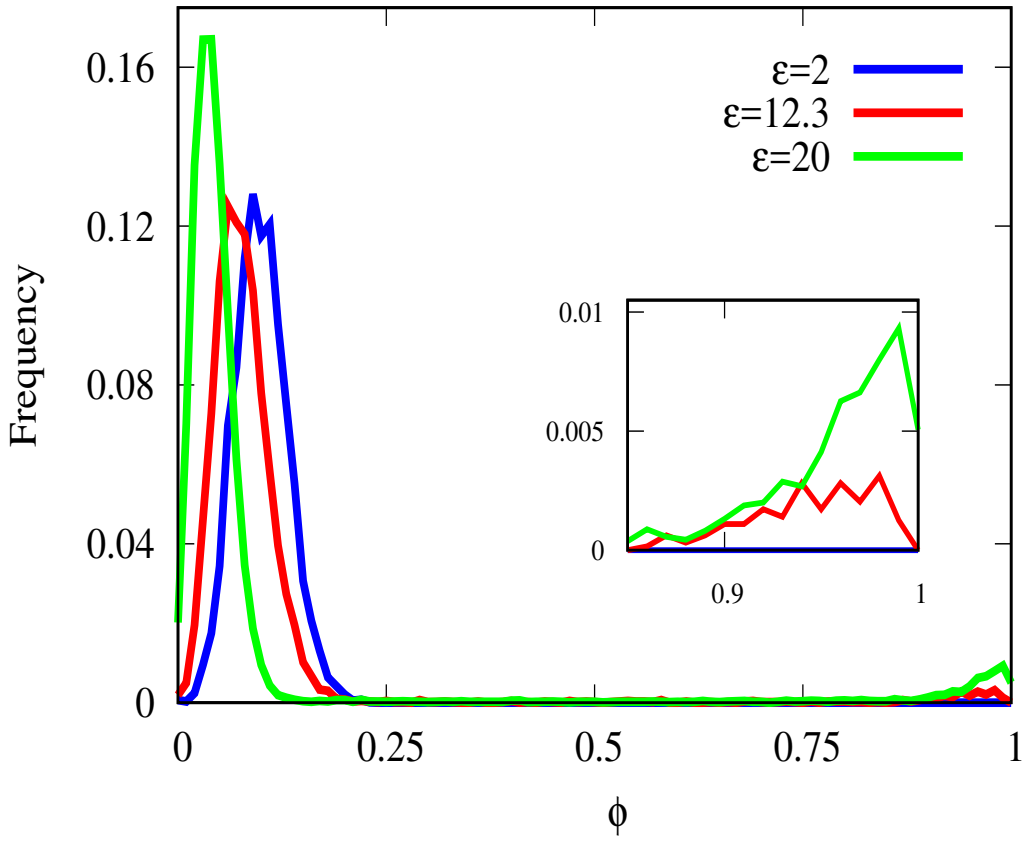

Figure 4.3: Density frequency histogram of a lattice $L = 200$ for $\rho = 0.1$ and $D_r = 0.1$ for three different activities. Red line represents the minimum activity needed for the phase separation.

a fixed density $\rho = 0.1$, a rotation coefficient $D_r = 0.1$ and multiple activities. The density frequency histogram was estimated by subdividing the lattice in small squares of size 10×10 and measure the local density through the entire lattice. Once all local densities are determined, we divided the counted number of a determined density by the total number of subdivisions of the lattice.

The results of the density frequency histograms for three different activities are shown in figure *4.3*. For small activity ($\varepsilon = 2$) the distribution is centered at 0.1, as expected since the system remains in the

dilute state, near the random walk regime. When we increase the activity to 12.3 the peak is displaced to the left, compared with the almost passive Brownian regime, meaning that there are some regions with lower density, and a small but non-negligible peak appears in regions of high-density, evidencing the formation of a compact cluster. When we increase even further the activity, two peaks emerge, a peak near zero and another near one, suggesting two complete distinct phases, one very dilute (near zero density) and another dense (the large majority of the particles form a compact cluster). A snapshot of a lattice resulting from numerical simulation for the final states of the three distinct activities is shown in figure 4.4, showing the agreement between the interpretation of the density frequency histogram and the system's configuration.

Since all dynamics are governed by particle diffusion and there are no interactions whatsoever between particles besides excluded volume, the only mechanism driving the phase separation is motility, therefore we are in the presence of a Motility Induced Phase Separation (MIPS). Although we confirmed that this model leads to MIPS, we still pursue a more precise evaluation of the threshold of activities leading to MIPS as a function of the number of particles in the system.

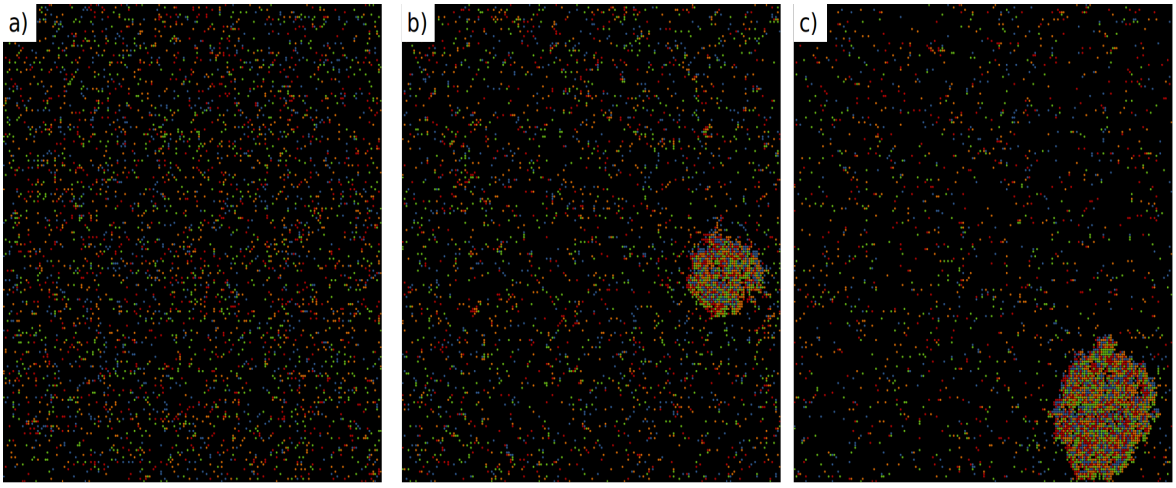

Figure 4.4: Snapshots of configurations of an active system with PBC for three different activities. a) $\varepsilon = 2$ typical brownian diffusion were particles are uniformly distributed in space; b) $\varepsilon = 12.3$ minimum activity leading to MIPS; c) $\varepsilon = 20$ asymptotic regime where a large dense region is formed

Density frequency histograms allow us to distinguish phases qualitatively although in a not-so-precise manner, therefore another measurement is necessary to distinguish for which parameters a phase separation occurs. Note that the plot of the density frequency histogram on the dilute state resembles a Gaussian distribution, and when it phase separates it elongates. The fourth-order Binder cumulant (B_4) [31] gives a quantitative value for the kurtosis of a function, and as seen from figure 4.3, in the passive Brownian regime the kurtosis of the density frequency histogram should be zero, since no peak appears on the high density regions and the function should be a Gaussian with mean value $\rho = 0.1$. When activity is increased, the frequency of densities changes shape and must increase it's kurtosis since we can identify a peak in a high density region. B_4 has as the following mathematical expression:

$$B_4 = 1 - \frac{1}{3}\frac{\langle(\phi-\rho)^4\rangle}{\langle(\phi-\rho)^2\rangle^2}, \tag{4.2}$$

where ϕ is the local density, and $< . >$ is the average. Measuring the value of the fourth order Binder cumulant at the final configuration for all the range of activities, allows us to determine precisely the threshold activities that lead to MIPS, since if the distribution is Gaussian the fourth order Binder cu-

mulant must be zero. As plotted on figure 4.5, for the same parameters as before we observe that for an activity $\simeq 12.3$ the Binder cumulant changes from zero to $\simeq -10$, concluding that it's at this activity that the MIPS occurs, in full agreement with both the density frequency histograms and images in figures 4.3 and 4.4 respectively.

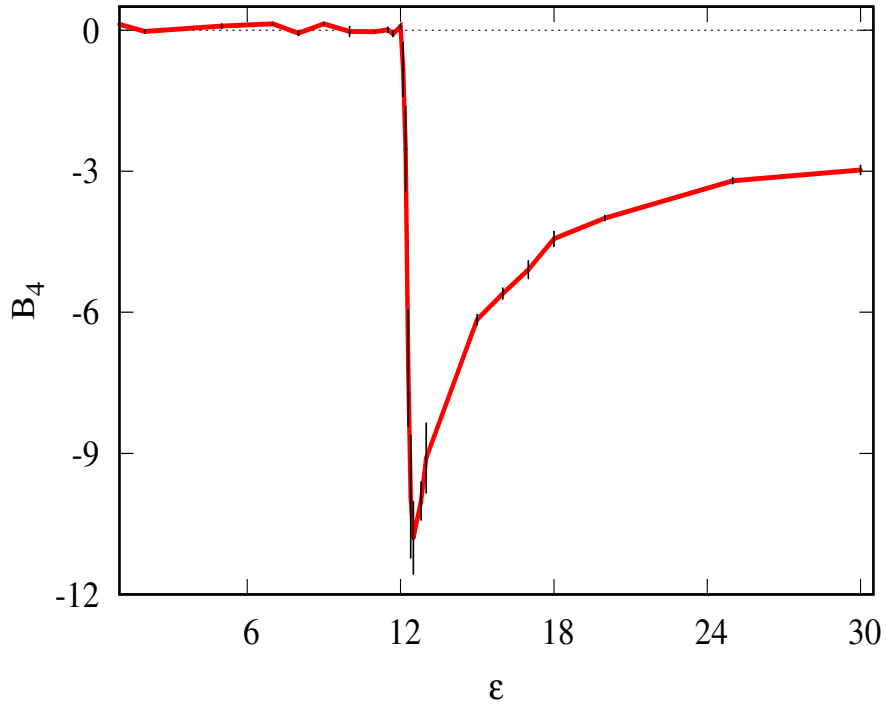

Figure 4.5: Fourth-order Binder cumulant as function of activity for $L = 200$, $\rho = 0.1$ and $D_r = 0.1$. Black dotted line represents $x = 0$. Black lines represent the error associated with the respective activity.

Besides examining B_4 as function of activity, we also measure its time evolution to ensure once more the validity of B_4 as a parameter to distinguish phases. All simulations start in a disordered state hence in the diluted phase. If B_4 is a valid parameter to distinguish the phase separation, then at the time where MIPS occurs, B_4 must change. A tempting idea would be to study time properties of MIPS, but from our tests we cannot determine precisely time properties of MIPS, since we only performed measurements in time intervals of powers of 2. Nonetheless, by observing figure 4.6 we can confirm the validity of B_4 as a parameter to characterise the phase transition, since the fourth-order Binder cumulant shifts from 0 to ~ -4 precisely at the time the system changes from the dilute to the coexistence regime, as represented in the inset. The large error bars at these time, arrive from the fact that some samples haven't yet phase separated and others have.

To study possible finite size effects, that is, if the results obtained are not effects arising from spatial limitations of the lattice, hence creating fictitious spacial correlations, we performed simulation for the same range of parameters on systems of size, $L = 200$, $L = 400$ and $L = 500$. Here we present in figure 4.7 the results obtained from the B_4 measurements for three different system sizes. From this plot, we can conclude that finite size effects emerge but are not relevant for the physical interpretation and validation of the results, since at constant density the activities leading to phase separation for different system sizes are consistent, as shown at the inset of figure 4.7.

Following the same line of thought used to describe MIPS for $\rho = 0.1$, we increased the system density ρ by 0.1 systematically from 0.1 to 0.5, and plotted the density histograms and the fourth or-

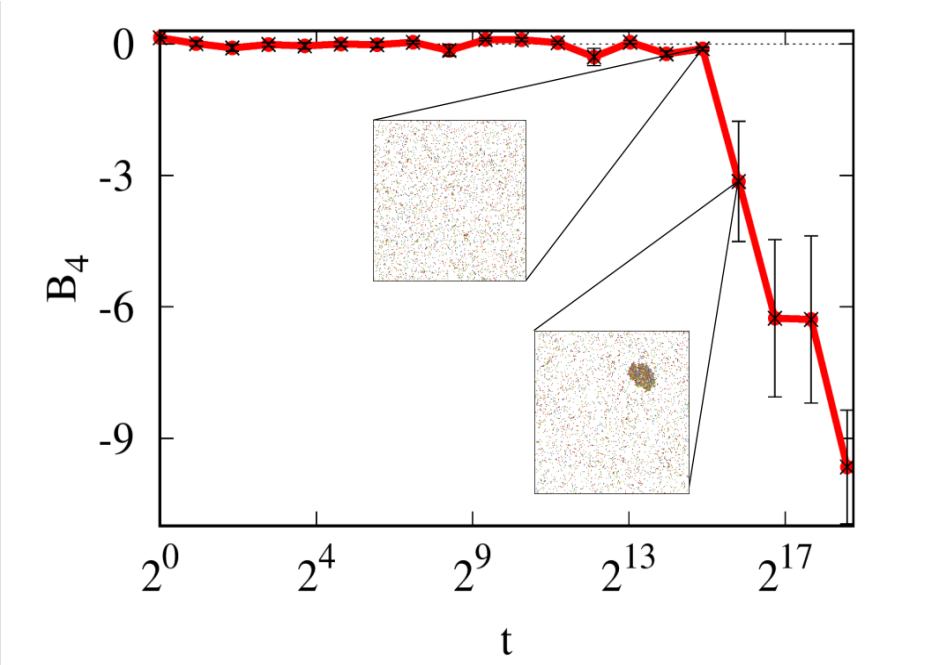

Figure 4.6: Time evolution of B_4 for parameters $\rho = 0.1$, $D_r = 0.1$ and $\varepsilon = 12.3$. Insets illustrate snapshots at the corresponding time.

der Binder cumulants. As expected from the flow arguments, at higher densities the minimum activity leading to MIPS decreases.

Distinguished the two regimes, one phase (dilute) and coexistence of two phases (dilute and dense), through the parameter activity, we plotted a phase diagram, shown in figure 4.8. Each point corresponds to the peak value of a density ϕ in the density frequency histogram, and as explained before and shown on figure 4.3, if it has one peak system just one phase exist, if it has two there is a coexistence of dilute and dense regions.

The phase diagram plotted on figure 4.8 represents a prediction of the final peaks of the frequency of densities knowing the initial conditions for the density ρ and activity ε. Given a system density ρ and an activity ε that fall inside the one phase region (in blue), the system will remain in a similar configuration to the initial, that is, the frequency of densities will only have one peak at $\phi \simeq \rho$. On the other hand, if the parameters ρ and ε are inside the coexistence, that is, any region of the red space of figure 4.8, the system will exhibit MIPS and have a corresponding frequency density histogram with two distinct peaks, where each value of the peak ϕ will be equal to the point of crossing of a horizontal line between the ε and the black dotted line represented in figure 4.8. The black dotted line is drawn by plotting the coexistence peaks of density $\rho = 0.5$, where it is theorized to exist a critical point [32, 33].

An important result we extract from the phase diagram is that the ρ does not determine the peaks of density frequency histogram when the system has a coexistence of two phases, but is rather the activity that sets the peaks. Observing the phase diagram we state that, independently of ρ, the dense and dilute phases are compacted similarly for an ε where MIPS occurs.

So far we have considered only the phase diagram for a fixed rotation rate $D_r = 0.1$. We proceed with the study of MIPS by increasing the rotation rate to $D_r = 0.2$, and follow the same steps as previously. At higher D_r, the time scale for a particle to change its self-propulsion direction lowers, therefore a phase separation is expected to occur at higher activities, since the average persistence length decreases and consequently the frequency of collision also decreases. Besides the smaller number of collision for

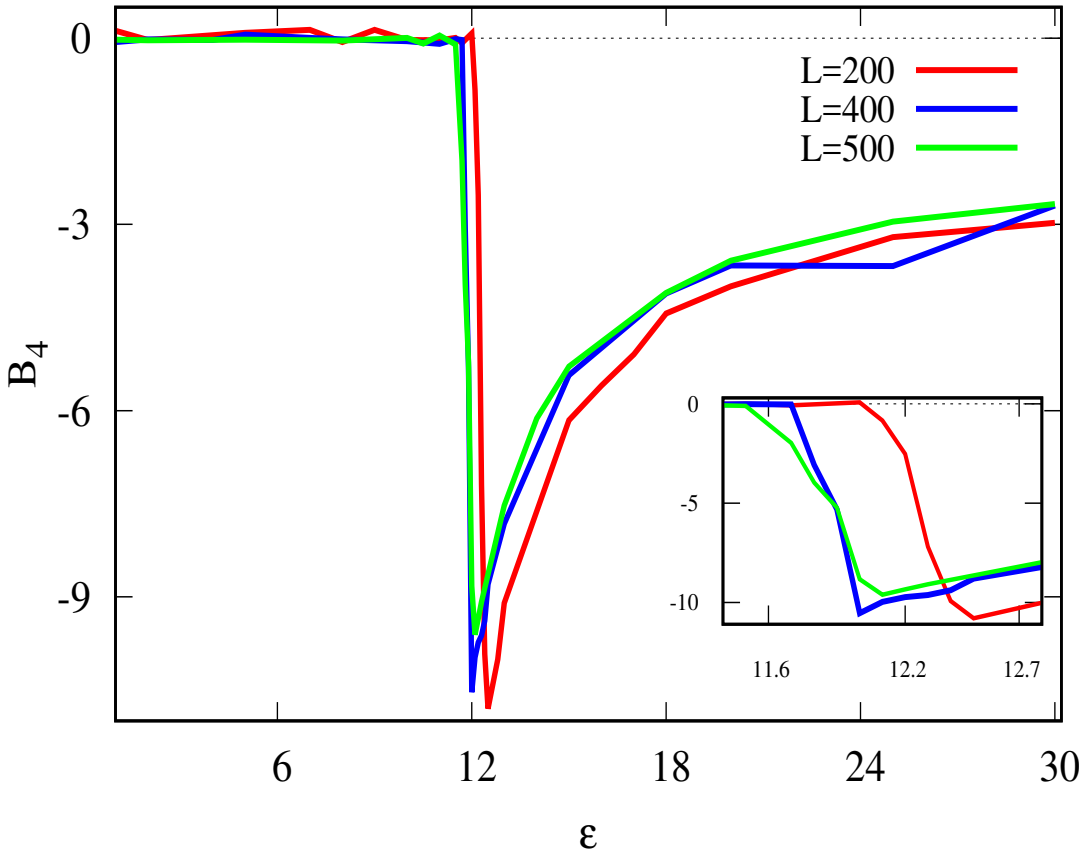

Figure 4.7: Finite size effects of B_4 as function of ε for system sizes of $L = 200$, $L = 400$ and $L = 500$. Inset represents a close up near the activity where MIPS is first observed. Black dotted line represents $x = 0$.

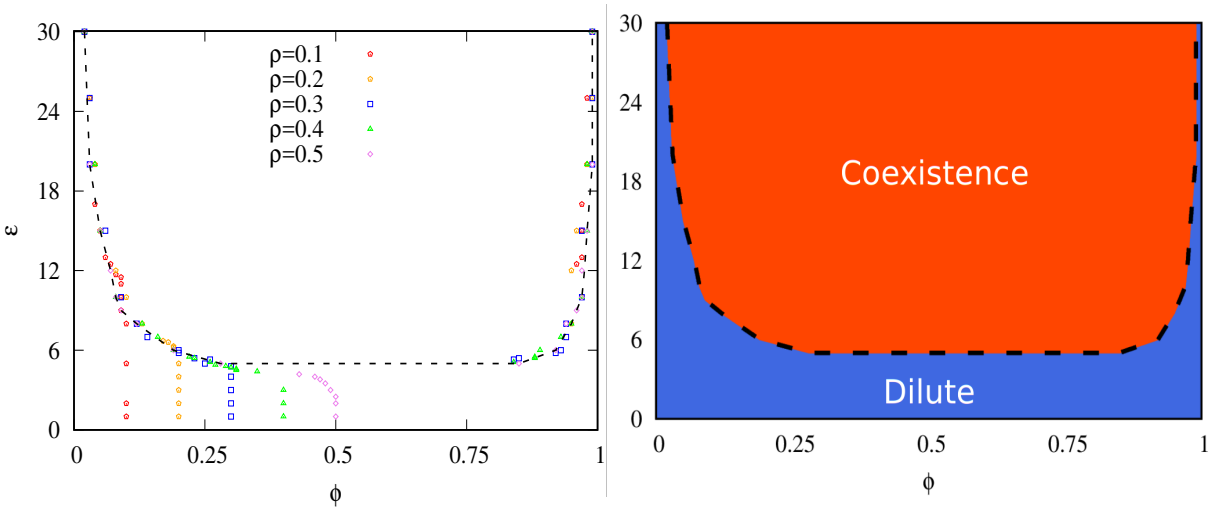

Figure 4.8: Activity ε vs density ϕ phase diagram for $L = 200$ and $D_r = 0.1$ for multiple system densities ρ. MIPS is observed for any activity ε and density ρ inside the red area.

higher D_r's, when particles cluster, the time scale for a particle to leave the forming cluster is smaller, thus the formation of two distinct phases is less likely.

The resulting phase diagram obtained from the numerical simulations at a higher coefficient rate on a lattice with size $L = 200$ are represented on figure 4.9. In this plot, we present only the activities were

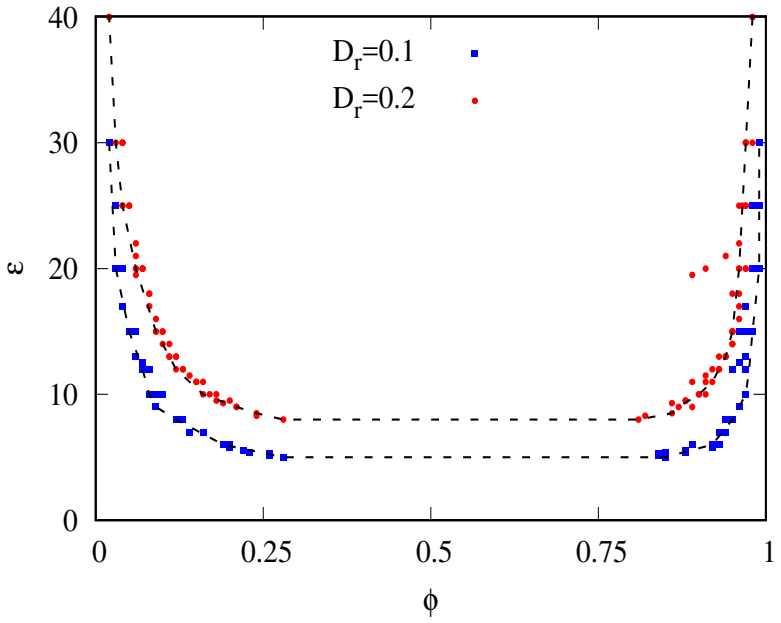

Figure 4.9: Activity ε vs density ϕ phase diagram of a lattice size $L = 200$ and both $D_r = 0.1$ and $D_r = 0.2$.. All points represent an activity where coexistence of phases occurs.

MIPS is observed for the same densities ρ ($[0.1 : 0.5]$) for two coefficient rates. It's clear that the line separating the coexistence is shifted upwards, demonstrating the fact that a higher activity is required for MIPS to occur. Another interesting result is the fact that the line separating the two regions is asymmetric independently of D_r.

4.3 Interfacial Properties

A point of interest and still an open discussion in the field of interfacial properties of active matter is to which universal class MIPS belongs to [34, 32]. We follow the work in [34], where it's studied the universality class of the interfacial growth. We present similar results and conclude that the interfacial roughening of a compact cluster of active matter belongs to the Edward-Wilkinson universality class.

We performed new numerical experiments, using the same numerical method described earlier in this chapter, and prepared a lattice with active Brownian particles with a set of parameters that was known to be inside the coexistence, that is, $\rho = 0.5$, $D_r = 0.1$ and $\varepsilon \geq 6$ (see figure 4.8). The main difference between the previous simulation and the presented now is in the initialisation of the lattice. Previously, in the initial state particles were randomly inserted, while now we set the initial configuration to be in a complete jammed state where all particles are compacted in one single cluster (*vide* figure 4.10). As the system evolves in time, the interface separating dilute and dense phases that was initially flat increases its roughness. Our focus is to classify the universal class of the interfacial growth.

The plots presented in figure 4.11 show the time evolution of the density of a column at distance $|x|$ from the centre of mass for different lattice sizes, rescaled by L. Initially there is a a vertical film at 0.25 where the presence of the interface clearly separates the two regimes, dilute (total absence of active particles from the initial conditions imposed) and dense. In the final state, the vertical film shifts to the left due to an outgoing initial flux of particles from the cluster, decreasing the total number of particles in the dense state and increasing the number of particles in the dilute state, setting the density in the dilute phase $\simeq 0.12$ as expected from the phase diagram in figure 4.8.

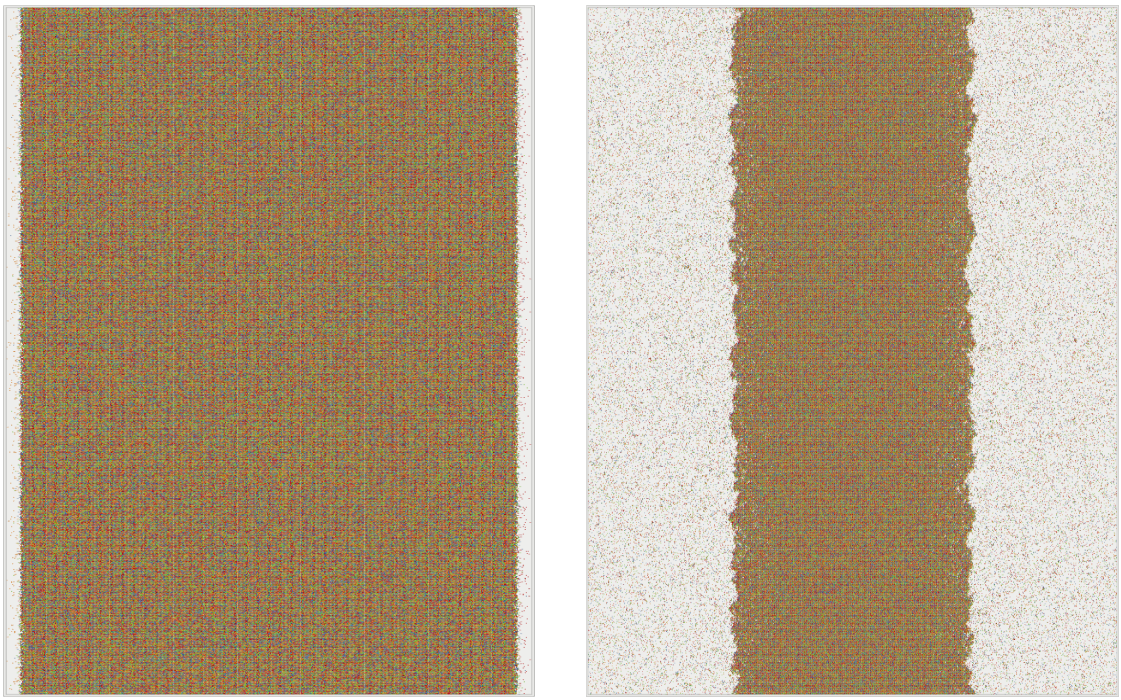

Figure 4.10: Initial and final configuration (left to right) of a system of size $L = 400$, $\rho = 0.5$ and $\varepsilon = 8$. Initial snapshot is zoomed in to the space occupied by the particles.

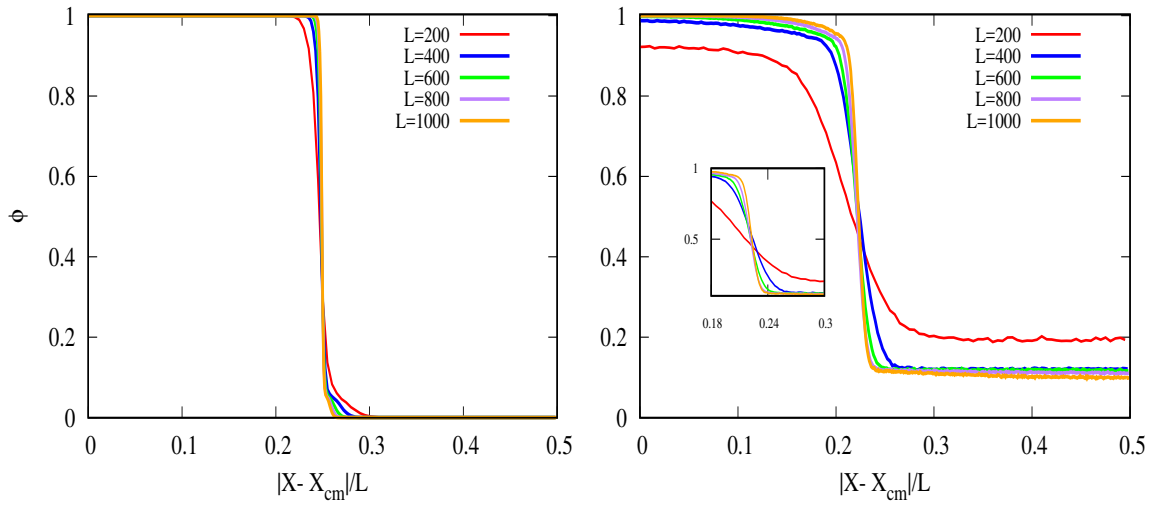

Figure 4.11: Local density time evolution (left to right) for different system sizes for $\rho = 0.5$ and $\varepsilon = 8$.

For all analyses of the interface and density distribution, we can consider the lateral interfaces uncorrelated and study them independently, therefore doubling the samples and resulting in better statistics. To comprehend why we can approximate them as independent, consider the initial state where particles fully occupy $\rho L_x L_y / L_x = L_y/2$ columns. In this configuration, the initial minimum distance between two points at the interfaces is $L_x/2$, when the density is $\rho = 0.5$. Knowing that the interface shortens the distance from the centre of mass because particles are only allowed to leave the initially flat cluster or rotate, the minimum distance between two points at the interfaces should decrease. We still have to consider the roughness increase, but from our measurements this increase does not compensate the shrinking of the cluster, concluding that we can consider both interfaces as independent.

Besides considering the macroscopic properties of the cluster, we need to account for the microscopic attributes of the active particles in order to consider the interfaces independent: The typical persistence length of the active particle must be less than the minimum distance between interfaces. When the activity is set to $\varepsilon = 8$, the average distance travelled by the particle in the self-propelled direction with a rotation coefficient $D_r = 0.1$ is $8/0.1 = 80$ lattice units. For this parameters (activity and rotation coefficient) MIPS is observed and are adequate to consider the interfaces uncorrelated because for the large systems, the average distance between the interfaces is always larger than 80. As for the smaller system ($L = 200$) it's plausible to assume that some finite size effects may play a relevant role, even though the activity is decreased to $\varepsilon = 6$, because it exhibits a different behaviour in figure 4.11. Independently of possible finite size effects, we can assume that the characteristic width of the interface is not influenced by the lattice size, since all points cross approximately the same point on figure 4.11.

To study if there is an universality class of the interfacial growth, we measured the time evolution of the roughness, as defined on chapter 3 equation 3.2. In the respective chapter we had a surface for particles to deposit, and in this section particles do not deposit on any structure, therefore we had to make an approximation of the definition of substrate. We defined the substrate as fictitious wall at $L_x/2$ and examined the average height and local fluctuations relative to this line for different system sizes.

Examining figure 4.12, where the growth of the interfacial roughness as function of KMC time is plotted, rescaled by L to the power of the characteristic exponents of EW university class (*vide* 3.2), we observe that for all system sizes the behaviour of the time evolution lines collapse, indicating that the interface roughness belongs to the universal class of EW. Besides overlapping, all curves follow the same power law, that is, they have the same exponent $\beta = \frac{1}{4}$. These results reveal that the interfacial growth of a system composed of active matter where it is known that MIPS will occur, if started in a fully compact rectangular configuration, is in the the Edward-Wilkinson universality class.

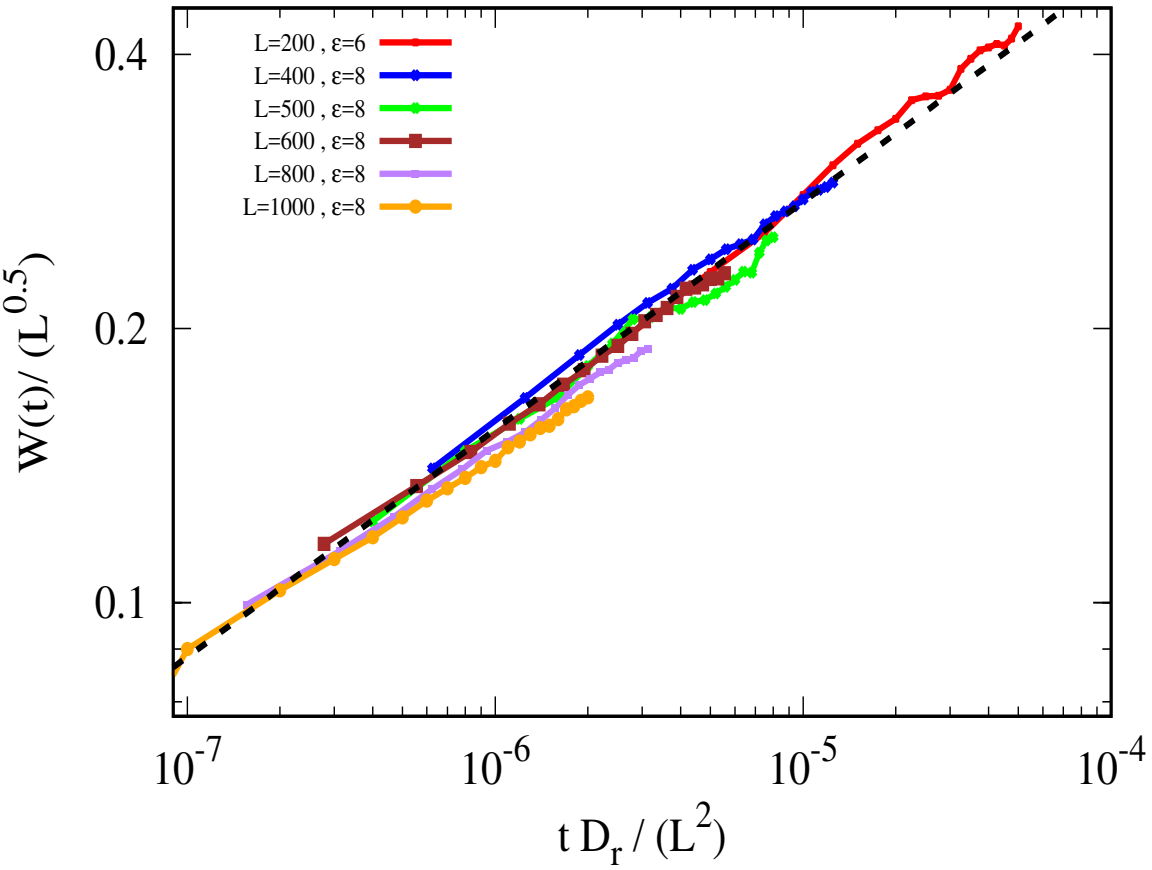

Figure 4.12: Interfacial roughness $W(t)$ for different system sizes. Data collapses when rescaled with EW exponents. Black dotted line represents $f(t) \sim t^{0.25}$

Chapter 5

With substrate

Aiming to study wetting transitions of active matter, a particular case of interfacial phase transition [35], we modified the Bulk model introduced in the previous chapter, introducing a constraint on the lattice, two walls on the *xx* boundaries, and kept the periodic boundary conditions on the *yy* direction.

Several question are still open on wetting transitions of active matter, such as if the phase diagram is affected by a confined geometry or what is the interfacial growth universal class. In this chapter we will elucidate and present results that will help understand some of these questions and further investigation.

In the following chapters, all simulations were performed using the KMC method analogous to that described in the Bulk section 4.2, and the burning method used to measure the roughness is analogous to the one described in the Random Deposition section 3.

5.1 "Canonical" Ensemble

In this section we investigate how activity and density in the canonical ensemble, that is, on a system with fixed number of particles at constant temperature, changes the dynamics of active matter. Up until now we have only considered lattices with periodic boundary conditions. Now, in the interest of investigating the influence of a substrate in self-organisation of the active particles, we add a lateral surface. Bulk and substrate results will be discussed via the analyses of both frequency density histograms and roughness.

In the presence of a substrate, a macroscopic dynamical constraint, we expect the active particles to aggregate throughout the wall, and hence, the morphology of the structure formed by the active matter is convenient to study the interfacial growth relatively to the wall, unlike in the previous chapter. Previously, the dense phase could assemble anywhere in the domain. Additionally from the random location of the cluster, we observed that depending on the number of particles, the cluster could have different morphologies, making difficult the analyses of the interfacial growth since we do not have a characteristic time for the cluster initial growth, which was highly computational demanding and time consuming.

As before, we start by a visual analysis and construct simple arguments for the phenomenology. Observing the images on figure 5.2, the main differences arising from an imposed wall constraint are location and geometry of the cluster formed, as expected. In the bulk, as seen in the top part of figure 5.2, the position of the cluster is not fixed and its geometry is not imposed by spacial restrictions, but in the presence of a substrate, particles always nucleate on the wall creating a non-uniform film, as represented on the lower part of figure 5.2. We can conclude then, that the cluster geometry is highly dependent on the physical constraints of the lattice.

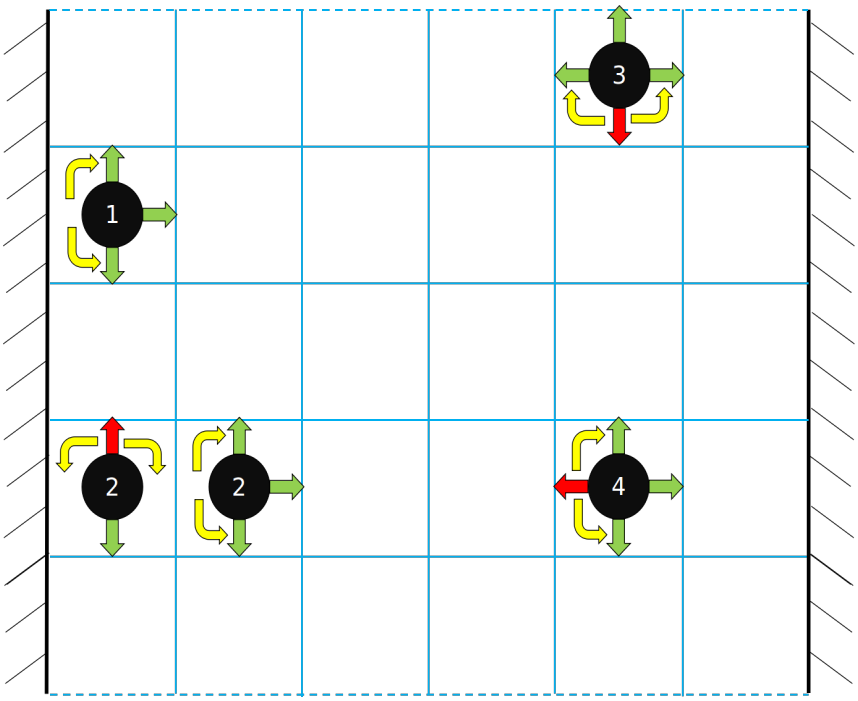

Figure 5.1: Representation of a semi-infinite with a lateral planar constraint lattice of size 6×5 with 5 active particles. The limits marked with dashed blue represent periodic boundary conditions and the black lines walls.

We want to understand how activity of the active particles leads to the formation of a film. Heuristically, we can use the same arguments as before and say that a film is only formed if the time scale for particle rotation is smaller than the time for another incoming particle to arrive at the substrate. We will follow the same line of thought as in bulk, that is, increase systematically the activity for different densities, in order to study the film properties.

Since we cannot compare bulk and wall spatial distributions due to the stochastic nature of the nucleation site of the cluster in the bulk, we measured the density frequency histograms, a distribution that allowed us to distinguish phases in the previous chapter, and investigate possible divergences from bulk and wall lattices. Observing figure 5.3 it is evident that for three different ρ's the density frequency histograms are identical for all activities, one outside the coexistence line, other near the coexistence point and one inside the coexistence with a large number of particles in the dense phase. This similarity indicates that there is a similarity between bulk MIPS and film formation.

A characteristic property of wetted substrates is the formation of a *plateau* in the density profile of the particles. In the plots presented in figure 5.4 we display the spatial density profiles and the roughness as function of Monte Carlo time, for a system of size $L_x = 500$ and $L_y = 300$. We only present the spatial density up to a distance of 120 lattice space units based on two arguments: first the system has already reached a constant density, and secondly, because we whish to consider the two walls independent and therefore the maximum distance of a particle to the wall is $L_x/2 = 250$.

We can consider the left and right wall as independent, if we make use of the same argumentation followed in the case of the initial cluster condition, discussed in the previous section. Observing the plots in figure 5.4, we can conclude that the interface maximum width is always smaller than 120 lattice space units. For the system under study, the maximum activity used was $\varepsilon = 20$ and the rotation coefficient was kept fixed at $D_r = 0.1$, therefore the average persistence length is 200 lattice space units. If we consider the limit of a film with a uniform width of 120 lattice space units on both sides, then the distance between

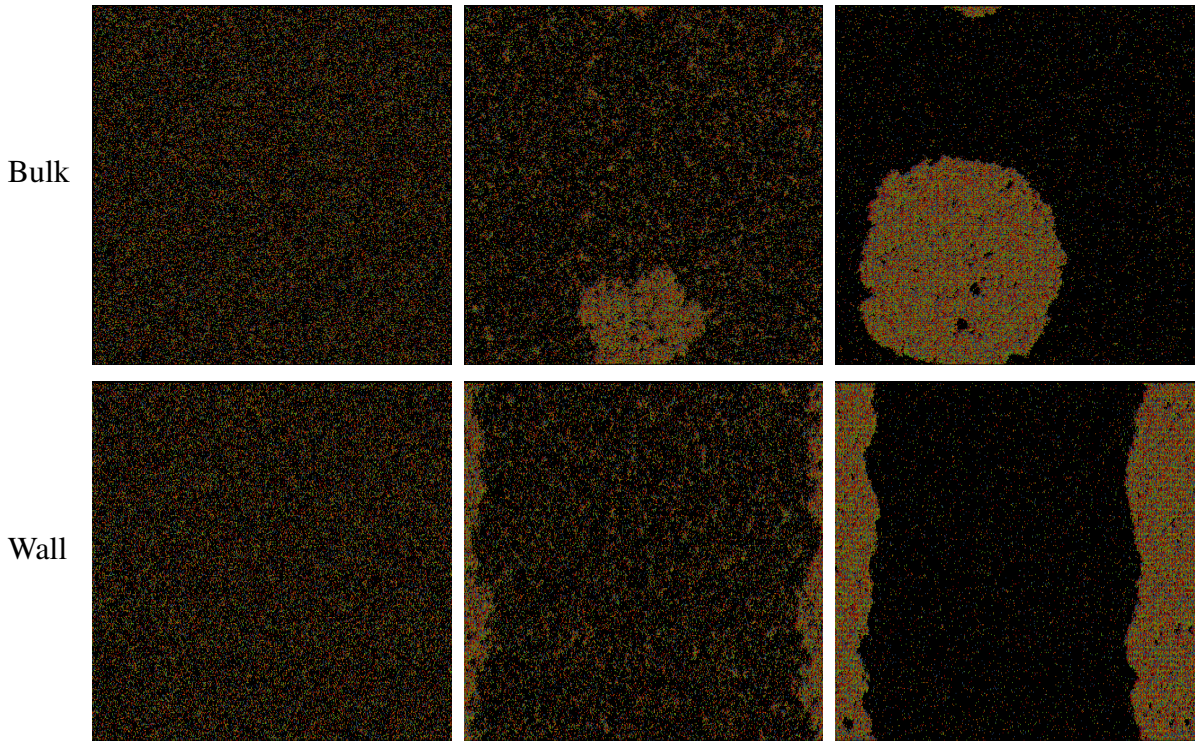

Figure 5.2: Snapshots of simulations at fixed density $\rho = 0.3$. Top and bottom correspond to bulk and wall, respectively, for three distinct activities. First activity on the left corresponds to single phase ($\varepsilon = 2$); Middle snapshots show an activity near the coexistence of two phases ($\varepsilon = 5.3$); Far right is for an activity $\varepsilon = 15$.

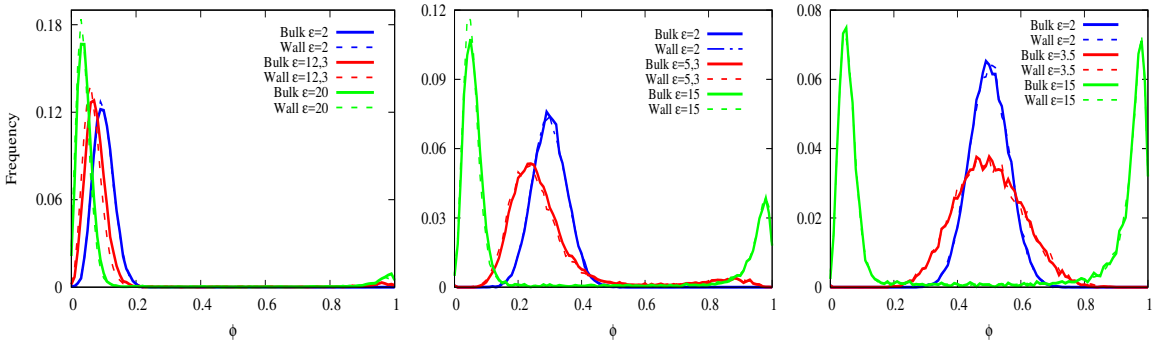

Figure 5.3: Comparison of the density frequency histograms between bulk and wall systems.a) $\rho = 0.1$; b) $\rho = 0.3$; c) $\rho = 0.5$

interfaces is 220, which is more than the average persistence length of the maximum activity. Since the film has a width smaller then 120, we can study both walls independent.

The results from the spatial density profile reveal that there is a characteristic size of the interface, given that for different times all density profiles intersect at the same point in space . Interestingly, even though the inflection point of the density spacial profile remains constant in time, the distribution of particles through the film starts to spread for times longer than 2^{14}. Since the film is not uniform but irregular, we could argue that in fact the film is not spreading but it is the roughness that is increasing. Looking at the plots of the time evolution of the roughness on figure 5.4, we observe that the roughness stays constant for Monte Carlo times $\geq 2^{10}$, and therefore the spreading of the film cannot be justified by the increasing roughness.

This change in behaviour of the long time limit of the film width can be due to two reasons. The first

is the change from the ballistic to the diffusion regime. In the long time limit , an isolated active particle changes regime from the purely ballistic to thermal diffusion [7]. Considering this regime change, what we observe is a loss of compactness due to the fact that the system is no longer on ballistic diffusion but on thermal one, consequently, the balance of the flux of the ingoing and outgoing of particles from the film decreases, leading to a decrease of the film width. The second reason is not due to a change in the diffuse regime but to a change in self-organisation of the deposited layers of the active particles, rearranging in a different configuration that reduces compactness, leading to the spreading of the film, but keeping the roughness constant.

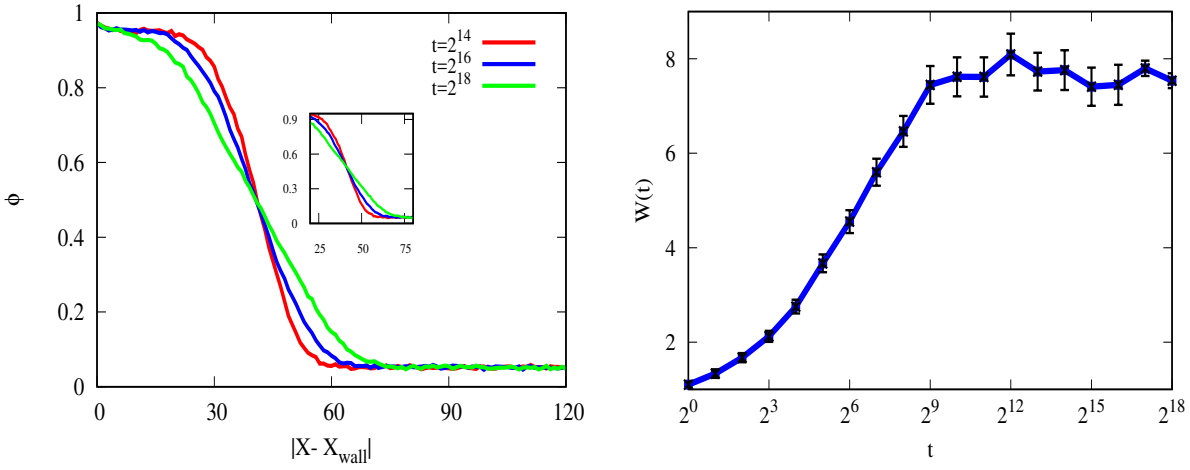

(a) System with $\rho = 0.2$ and $\varepsilon = 15$. Density profile, with inset for the crossing point of different times (left) and roughness as a function of Monte Carlo time (right), black lines represent error lines.

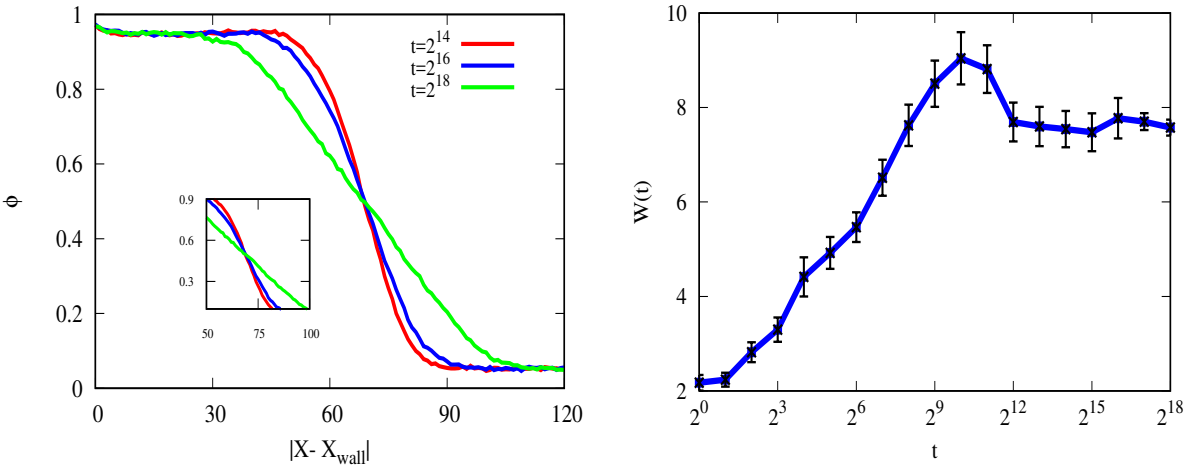

(b) System with $\rho = 0.3$ $\varepsilon = 15$. Density profile, with inset for the crossing point of different times (left) and roughness as a function of Monte Carlo time (right), black lines represent error lines

Figure 5.4: Plots of the density profiles and of the roughness for $\rho = 0.2$ and $\rho = 0.3$, for the same activity $\varepsilon = 15$.

As previously done, both in chapters 3 and 4.2, we evaluated the surface growth and its scaling properties. We found that the exponents that characterise the surface growth do not follow any of the power laws of any of the universality classes studied, so we deduce that the EW universal class that characterises the surface growth in the Marchetti model ([34]) are dependent on the initial state.

5.2 “Grand Canonical” Ensemble

In the previous section we studied how the interface of a collection of active particles develops in semi-infinite system for a fixed number of particles, and concluded that the power laws of the time evolution of the roughness do not corresponded to any universality class of our knowledge. One of the reasons for the saturation regime of the roughness, results from the insufficient number of particles in the bulk that limits the flux of incoming particles .

When we restrict the number of particles to a fixed quantity, the bulk region is depleted when particles start to deposit on the substrate. Looking at figure 4.8, where we show the phase diagram of MIPS, when density is locally decreased, we leave the two phase region and can no longer expect particles to continue to accumulate on the surface. So the question is, what would happen if we had an infinite number of particles so that we could keep the system density fixed at coexistence in the bulk, and a small surface for particles to deposit, that is, if the substrate was inserted in an infinite reservoir do the roughness properties change.

The challenge in implementing a grand canonical ensemble is the technical difficulty of developing a numerical model of a large lattice with a large number of particles that runs in a practical time. Therefore we need to make some approximations in order to mimic a substrate immersed in a particle reservoir without resorting to a large lattice space and an endless number particles.

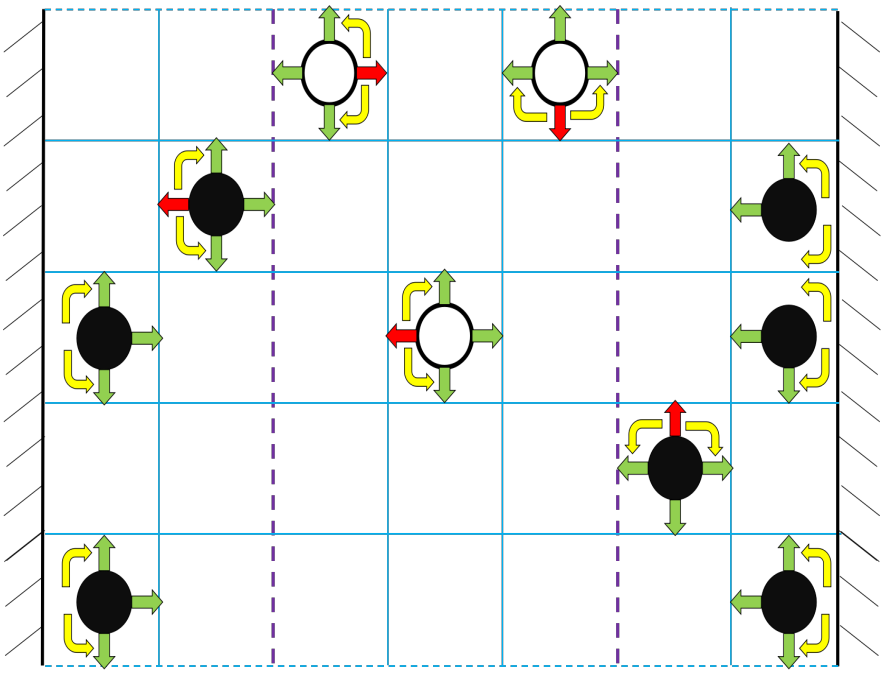

Figure 5.5: Representation of a lattice with initial $\rho = 0.2$. Bulk is simulated between the dashed purple lines. Black particles are initially inserted, white ones are introduced to keep the bulk density fixed

With the goal of describing a grand canonical ensemble with two substrates in it, we set a finite lattice with two walls separated by L_x, but kept the periodic boundary conditions in the yy direction. The first approximation is to consider the bulk region as an area at some equally predetermined distanced from both walls. We then let the system evolve until a Monte Carlo time $t \geq 2^9$, where the roughness stops increasing and starts to saturate (*vide* figure 5.4). Since our argument for the saturation regime was the lack of incoming particles from the bulk, we then measure the system density in the bulk, and if it is lower than that initially imposed, we insert particles periodically until it attains the initial density.

5. WITH SUBSTRATE

Since particles can be inserted systematically, it can lead to an over saturation regime, and so, to prevent this we also consider the possibility of removing particles with the same periodicity as they are inserted, when the density is higher than that initially imposed. Since particles can be inserted and removed, we consider this an approximation to the grand canonical ensemble.

As in previous chapters, we inserted a timing stop condition. In this simulations, besides stopping for times longer than $t = 2^{18}$, we also inserted a restriction for the total number of particles, that is, if the lattice density is above to ρ_{max} we stop the simulation. The ρ_{max} is set to guarantee that for the activity under consideration we can consider both walls independent, and so, when the total density of the system is such that, if all particles were part of the film, we could no longer consider walls as independent, we stop the simulation to prevent correlations between the interfacial growth at the two surfaces.

A result worth mentioning is that, from our simulations, the only stopping condition applied was the ρ_{max} one, meaning that particles were inserted most of the time.

We are now interested in studying the universality class of the roughness of the growing interface for this approximate grand canonical ensemble. We performed simulation for different L_y sizes keeping the rotation rate fixed at $D_r = 0.1$, as in the previous models, for three different densities ($\rho = 0.1$, $\rho = 0.2$ and $\rho = 0.3$). For all three ρ's studied, activity was chosen so that we are at the two phases regime.

From the measurements taken of the roughness as function of the number of deposited layers for different system sizes, we rescaled both axis by the wall size to the power of the universal class exponents previously presented, but it failed to collapse, indicating that the non-equilibrium roughening presented here does not belong to any of the previously studied universal classes. We then rescaled by the characteristic exponents of KPZQ and all lines collapse, indicating that this is the appropriate universality class for the grand canonical ensemble of active matter.

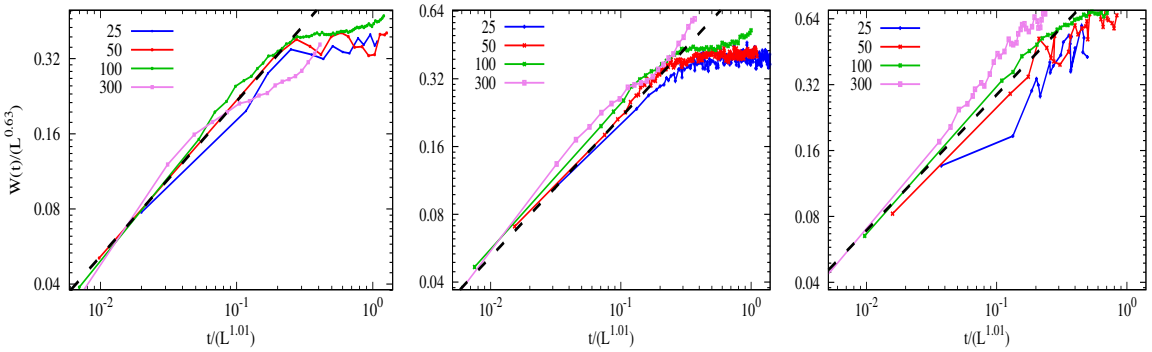

Figure 5.6: Roughness for three different densities ρ = 0.1, ρ = 0.2, and ρ = 0.3 (left to right) for the corresponding activities $\varepsilon = 12.3$, $\varepsilon = 6.7$ and $\varepsilon = 5.3$. Time t measured in terms of deposited layers. Black dotted line represents $f(t) \sim t^{0.62}$

Chapter 6

Conclusion

The growth of films and their interfacial properties, under far-from-equilibrium conditions, is a wide area of statistical physics with a lot to unveil. In this work, we developed stochastic models that characterise how collective behaviour develops structures, and try to understand it trough statistical methods, to identify the universality class of the interfacial roughness.

In this thesis, we approached the physical problems using numerical tools. We started on chapter 2 by implementing a computational technique, Kinetic Monte Carlo, which helped us study the growth of films under non-equilibrium conditions. KMC is a rejection free method, therefore a fast method, with practical applications since it can describe time evolution. We then used this model to study three non-equilibrium deposition models and simulate active matter systems with different spatial constrains.

The first three non-equilibrium growth models, studied in the third chapter, are associated with particle deposition. This chapter has as objective validate numerical methods and results, using the theoretical work done by Barabasi [24]. Each of the models studied, Random Deposition, Random Deposition with Surface Relaxation and Ballistic Deposition, belong to distinct universality classes for the time evolution of the interfacial roughness. For the first model studied, Random Deposition, we verified, through analytical tools and numerical verification, that the roughness grows indefinitely with the number of deposited layers with a characteristic exponent $\beta = \frac{1}{2}$. In the second model, Random Deposition with Surface Relaxation, were local lateral correlations are introduced, we also verified, using both analytical and numerical results, that the roughness of the growing interface belongs to the Edward-Wilkinson universality class. In the last model of non-equilibrium roughening, Ballistic Deposition, we use numerical results to verify the KPZ universal class, the class to which this model belongs to.

In the fourth chapter we begin the study of collective behaviour of active matter in the bulk. We used KMC method to implement numerical simulations of a collection of hard active particles, and study the Motility Induced Phase Separation. The central goal of this fourth chapter is to determine how density, activity and rotational diffusion affect the self-organisation of active particles. For a range of these parameters, we measured frequency density histograms, enabling us to distinguish two phases, a single phase were active matter is uniformly distributed in space, and a two phase system, were a compact cluster is formed around a dilute region. To ensure the validation of the results obtained from the frequency density histograms, we measured the corresponding fourth order Binder cumulant as function of both time and activity for different system sizes, and in fact there was a good agreement between the obtained results. Finite size effects were also studied through repeating simulations for larger system sizes, and no relevant effects emerged, validating the results obtained. Having set the range of parameters that lead to MIPS, we computed a phase diagram. From this phase diagram, we can predict from the set initial conditions (density ρ, activity ε and rotation coefficient D_r), the densities, either of the single

phase or the two phase regime, thus if MIPS is going to occur or not.

The final work presented on the fourth chapter, follows the work of [34], and investigates the roughness of active matter interface, starting with a compact cluster in the two phase region, which relaxes to the coexistence density at that activity. We found, by studying different system sizes and using the appropriate exponents, that the roughness belongs to the universality class of the Random Deposition with Surface Relaxation, that is, the Edward-Wilkinson class.

In the last section of this thesis, we studied two numerical models of active matter in a confined geometry, one where the number of particles is kept fixed, and another where the number of particles changes in time. In the first model, N fixed ensemble, we found a relation between MIPS and the nucleation of particles onto the substrate, by comparing the density frequency histograms for multiple values of density ρ and activity ε and observing that the distribution is similar for both cases. We also concluded that a planar confining geometry, changes the morphology of a self-organised cluster composed of active particles, by distributing them along the wall in a rough film. With the second set of simulations, we studied the roughness as function of the number of deposited layers and found that it belongs to the KPZQ universal class.

As an overall review, in this thesis we used numerical models to study far for equilibrium growing phenomena for particle deposition, and also phase separation active matter. For the active matter we were able to compute a phase diagram for MIPS, and found two different universality classes for the roughening growth of the interface of active matter.

Bibliography

[1] Manuel Schaffner, Patrick A. Rühs, Fergal Coulter, Samuel Kilcher, and André R. Studart. 3D printing of bacteria into functional complex materials. *Science Advances*, 3, 2017.

[2] This Month in Physics History.

[3] Brownian motion — physics — Britannica.com.

[4] Albert Einstein. Motion of suspended particles on the kinetic theory. *Annalen der Physik*, 1905.

[5] Jean Perrin. Mouvement brownien et réalité moléculaire. *Ann. Chim. Phys.*, 1909.

[6] Christian Scholz, Michael Engel, and Thorsten Pöschel. Rotating robots move collectively and self-organize. *Nature Communications*, 9:931, 2018.

[7] Clemens Bechinger, Roberto Di Leonardo, Hartmut Löwen, Charles Reichhardt, Giorgio Volpe, and Giovanni Volpe. Active Particles in Complex and Crowded Environments. 2016.

[8] Giorgio Volpe, Giovanni Volpe, and Sylvain Gigan. Brownian Motion in a Speckle Light Field: Tunable Anomalous Diffusion and Selective Optical Manipulation. *Scientific Reports*, 4:3936, 2015.

[9] Stanislaw Makarchuk, Vasco C. Braz, Nuno A. M. Araújo, Lena Ciric, and Giorgio Volpe. Enhanced propagation of motile bacteria on surfaces due to forward scattering. 2019.

[10] Stephen Whitelam, Katherine Klymko, and Dibyendu Mandal. Phase separation and large deviations of lattice active matter. *The Journal of Chemical Physics*, 148:154902, 2018.

[11] Stephen Whitelam. Individual and collective properties of lattice-based active particles. 2017.

[12] Michael E. Cates and Julien Tailleur. Motility-Induced Phase Separation. *Annual Review of Condensed Matter Physics*, 6:219–244, 2015.

[13] D M Woolley. Motility of spermatozoa at surfaces. *Reproduction (Cambridge, England)*, 126:259–70, 2003.

[14] Néstor Sepúlveda and Rodrigo Soto. Universality of active wetting transitions. 2018.

[15] Edward N. Lorenz. Deterministic Nonperiodic Flow. *Journal of the Atmospheric Sciences*, 20:130–141, 1963.

[16] Stephen Lynch. *Dynamical Systems with Applications Using Mathematica®*. Springer International Publishing, Cham, 2017.

[17] Millennium Problems — Clay Mathematics Institute.

[18] Davide Castelvecchi and Alexandra Witze. Einstein's gravitational waves found at last. *Nature*, 2016.

[19] Dirk Helbing, Illés Farkas, and Tamás Vicsek. Simulating dynamical features of escape panic. *Nature*, 407:487–490, 2000.

[20] Carlos Vázquez. An upwind numerical approach for an American and European option pricing model. *Applied Mathematics and Computation*, 97:273–286, 1998.

[21] Robert H. Silsbee and Joerg Draeger. *Simulations for solid state physics : an interactive resource for students and teachers*. Cambridge University Press, 1997.

[22] Nicholas Metropolis, Arianna W. Rosenbluth, Marshall N. Rosenbluth, Augusta H. Teller, and Edward Teller. Equation of State Calculations by Fast Computing Machines. *The Journal of Chemical Physics*, 21:1087–1092, 1953.

[23] Alfred B. Bortz, Malvin .H. Kalos, and Joel L. Lebowitz. A new algorithm for Monte Carlo simulation of Ising spin systems. *Journal of Computational Physics*, 17:10–18, 1975.

[24] Albert-Laszlo. Barabasi and H. Eugene (Harry Eugene) Stanley. *Fractal concepts in surface growth*. Press Syndicate of the University of Cambridge, 1995.

[25] Lutz Niemeyer, Luciano Pietronero, and Hans J. Wiesmann. Fractal Dimension of Dielectric Breakdown. *Physical Review Letters*, 52:1033–1036, 1984.

[26] Fractals, scaling and growth far from equilibrium. *Choice Reviews Online*, 1998.

[27] Hans J. Herrmann, D C Hong, and H E Stanley. Backbone and elastic backbone of percolation clusters obtained by the new method of 'burning'. *Journal of Physics A: Mathematical and General*, 17:L261–L266, 1984.

[28] Nuno Miguel Azevedo Machado de Araújo. Kinetics of deposition and post evolution relaxation in thin-films. 2009.

[29] Francis F. Chen. Diffusion and Resistivity. In *Introduction to Plasma Physics and Controlled Fusion*, pages 145–185. Springer International Publishing, Cham, 2016.

[30] Giorgio Volpe, Sylvain Gigan, and Giovanni Volpe. Simulation of the active Brownian motion of a microswimmer. *American Journal of Physics*, 82:659–664, 2014.

[31] Kurt Binder. Critical Properties from Monte Carlo Coarse Graining and Renormalization. *Physical Review Letters*, 47:693–696, 1981.

[32] Benjamin Partridge and Chiu Fan Lee. Critical motility-induced phase separation belongs to the Ising universality class. 2018.

[33] Juliane U. Klamser, Sebastian C. Kapfer, and Werner Krauth. Thermodynamic phases in two-dimensional active matter. *Nature Communications*, 9:5045, 2018.

[34] Adam Patch, Daniel M. Sussman, David Yllanes, and M. Cristina Marchetti. Curvature-dependent tension and tangential flows at the interface of motility-induced phases. *Soft Matter*, 14:7435–7445, 2018.

[35] Margarida M. Telo da Gama. Theory of Wetting and Surface Critical Phenomena. In *Computer Simulations of Surfaces and Interfaces*, pages 239–258. Springer Netherlands, Dordrecht, 2003.

[36] Cristóvão de Sousa Dias. Kinetics of thin-film mass transport on crystalline and amorphous substrates. 2011.

[37] Kim Christensen and Nicholas R Moloney. *Complexity and Criticality*, volume 1 of *Imperial College Press Advanced Physics Texts*. Imperial College Press, 2005.

[38] Masao Doi. *Soft matter physics.* Oxford University Press USA, 2013.

Appendices

Appendix A

Random Variable Properties

The motion of colloidal particles suspended in a fluid follow Brownian dynamics, that is, the macroscopic particles that are inserted into the fluid, experience successive random collisions with the microscopic particles that constitute the fluid, creating a phenomena similar to a random walk. As a consequence of these successive collisions, the suspended particles suffer a dragging effect, dependent on the fluid's viscosity, causing them to move in random directions. This dynamics can then be described phenomenological by the overdamped Langevin's equation:

$$m\frac{\partial v(t)}{\partial t} = -\gamma v(t) + \eta(x,t), \tag{A.1}$$

where γ is the friction coefficient of fluid, m the mass, and $\eta(x,t)$ the stochastic term that describes the force exerted on the particle by the multiple collisions with the fluid molecules. Although these collisions are random, some statistical properties need to be imposed in order to correspond to the physical constraints:

1. η obeys a Gaussian distribution
2. $\langle \eta(x,t) \rangle = 0$
3. $\langle \eta(x_i,t)\eta(x_j,t') \rangle = 2D\delta(x_i - x_j)\delta(t-t')$

The first condition is due to the fact that particle velocity distribution must follow a Maxwell-Boltzmann distribution. Secondly we impose the mean value of the random variable as 0, to simulate the equal probability of the particle going in any direction at any time. Finally, the third condition describes the temporal and spatial uncorrelation between two stochastic values, which represents the independence of the changes in velocity at different times in different locations, and sets the thermal diffusion coefficient D to

$$D = 2\gamma k_B T \tag{A.2}$$